

# Analysis of atmospheric ammonia over South and East Asia based on the MOZART-4 model and its comparison with satellite and surface observations

Pooja V. Pawar<sup>1\*</sup>, Sachin D. Ghude<sup>1</sup>, Chinmay Jena<sup>1</sup>, Andrea Möring<sup>2,7</sup>, Mark A. Sutton<sup>2</sup>, Santosh Kulkarni<sup>3</sup>, Deen Mani Lal<sup>1</sup>, Divya Surendran<sup>4</sup>, Martin Van Damme<sup>5</sup>, Lieven Clarisse<sup>5</sup>, Pierre-François Coheur<sup>5</sup>, Xuejun Liu<sup>6</sup>, Gaurav Govardhan<sup>1</sup>, Wen Xu<sup>6</sup>, Jize Jiang<sup>7</sup>, and Tapan Kumar Adhya<sup>8</sup>

<sup>1</sup>Indian Institute of Tropical Meteorology (IITM), Pune, 411008, India

<sup>2</sup>Centre for Ecology & Hydrology (CEH), Edinburgh, EH26 0QB, UK

<sup>3</sup>Centre for Development of Advanced Computing, Pune, 411008, India

<sup>4</sup>Indian Meteorological Department (IMD), Pune, 411005, India

<sup>5</sup>Université libre de Bruxelles (ULB), Spectroscopy, Quantum Chemistry and Atmospheric Remote Sensing (SQUARES), Brussels, B-1050, Belgium

<sup>6</sup>College of Resources and Environmental Sciences, National Academy of Agriculture Green Development, China Agricultural University, Beijing 100193, China

<sup>7</sup>The University of Edinburgh, Scotland, EH8 9AB, UK

<sup>8</sup>Kalinga Institute of Industrial Technology, Bhubaneswar, 751016, India

Correspondence to: Sachin D. Ghude (sachinghude@tropmet.res.in)

**Abstract.** Limited availability of atmospheric ammonia (NH<sub>3</sub>) observations, limits our understanding of controls on its spatial and temporal variability and its interactions with ecosystems. Here we used the Model for Ozone and Related chemical Tracers (MOZART-4) global chemistry transport model and the Hemispheric Transport of Air Pollution version-2 (HTAP-v2) emission inventory to simulate global NH<sub>3</sub> distribution for the year 2010. We presented a first comparison of the model with monthly averaged satellite distributions and limited ground-based observations available across South Asia. The MOZART-4 simulations over South Asia and East Asia were evaluated with the NH<sub>3</sub> retrievals obtained from the Infrared Atmospheric Sounding Interferometer (IASI) satellite and 69 ground based monitoring stations for air quality across South Asia, and 32 ground based monitoring stations from the Nationwide Nitrogen Deposition Monitoring Network (NNDMN) of China. We identified the northern region of India (Indo-Gangetic Plain, IGP) as a hotspot for NH<sub>3</sub> in Asia, both using the model and satellite observations. In general, a close agreement was found between yearly-averaged NH<sub>3</sub> total columns simulated by the model and IASI satellite measurements over the IGP, South Asia (r=0.81) and North China Plain (NCP), of East Asia (r=0.90). However, the MOZART-4 simulated NH<sub>3</sub> column was substantially higher over South Asia than East Asia, as compared with the IASI retrievals, which show smaller differences. Model simulated surface NH<sub>3</sub> concentrations indicated smaller concentrations in all seasons than surface NH<sub>3</sub> measured by the ground based observations over South and East Asia, although uncertainties remain in the available surface NH<sub>3</sub> measurements. Overall, the comparison of East Asia and South Asia using both MOZART-4 model and satellite observations showed smaller NH<sub>3</sub> columns in East Asia compared with South Asia for comparable emissions, indicating rapid dissipation of NH<sub>3</sub> due to secondary aerosol formation, which can be explained by larger emissions of acidic precursor gases in East Asia.

## 1 Introduction

Gaseous pollution due to various forms of nitrogen emissions plays an important role in environmental processes. Specifically, ammonia ( $\text{NH}_3$ ) emitted from various agricultural activities, such as use of synthetic fertilizers, animal farming, etc., together with nitrogen oxides ( $\text{NO}_x$ ) is one of the largest sources of reactive nitrogen ( $\text{Nr}$ ) emission to the atmosphere. Ammonia has great environmental implications due to its substantial influence on the global nitrogen cycle and associated air pollution, ecosystem and on public health (Behera et al., 2013; Liu et al., 2017b; Zhou et al., 2016). Emission estimates provided by latest EDGAR v4.3.2. emission inventory suggests that globally about 59 Tg of  $\text{NH}_3$  was emitted in the atmosphere in 2012 out of which agricultural soils contributed about 56 %, manure management contributed about 19 %, and agricultural burning contributed about 1.5 % (Crippa et al., 2018). Ammonia is a key precursor in aerosol formation, as the reactions in the atmosphere lead to an increase in different forms of sulphates and nitrates that contribute in secondary aerosol formation (Pinder et al., 2007, 2008). India and China together accounted for an estimated 64 % of the total amount of  $\text{NH}_3$  emissions in Southern Asia during 2000-2014 (Xu et al., 2018). Emissions of  $\text{NO}_x$  and  $\text{NH}_3$  are increasing substantially over South Asia (Sutton et al., 2017), which contributes to increase in particulate mass loading, visibility degradation, acidification and eutrophication (Behera et al., 2013; Ghude et al., 2008, 2013, 2016). Asia is responsible for the largest share of global  $\text{NH}_3$  emissions (Janssens-Maenhout et al., 2012). Further increase in  $\text{NH}_3$  emission will increase its negative impacts and societal cost (Sutton et al., 2017).

In India, around 50 % of total  $\text{NH}_3$  emissions is estimated from the fertilizer application and remaining from livestock and other  $\text{NH}_3$  sources (Aneja et al., 2011; Behera et al., 2013). However, there are large uncertainties in emissions of ammonia, its deposition to surface, chemistry and transport (Sutton et al., 2013; Zhu et al., 2015). Urea is mostly used as a fertilizer (Fertilizer Association of India annual report 2018-19) and alone contributes more than 90 % of total fertilizer used for the agricultural activities (Sharma et al., 2008). India is currently the second largest consumer of fertilizers after China, and fertilizer usage is bound to increase with further intensification of agriculture and the fertilizer input of India is expected to be doubled by 2050 (Alexandratos and Bruinsma, 2012).

Recent study based on Infrared Atmospheric Sounding Interferometer (IASI) satellite measurements show very high concentration of  $\text{NH}_3$  over Indo-Gangetic Plain (IGP) and North China Plain (NCP) which were mainly related to agricultural (Van Damme et al., 2014a, 2014b, 2015b) and industrial activity (Clarisse et al., 2019; Van Damme et al., 2018). The seasonality was shown to be more pronounced in the northern hemisphere, with peak columns in spring and summer season (Van Damme et al., 2014a). Van Damme et al., (2015a) attempted first to validate IASI- $\text{NH}_3$  measurements using existing independent ground-based and airborne data sets. This study doesn't include comparison of ground-based  $\text{NH}_3$  data sets with IASI measurements particularly over South Asia (India) due to limited availability of  $\text{NH}_3$  measurements. Liu et al. (2017a) estimated the ground-based  $\text{NH}_3$  concentrations over East Asia, combining IASI- $\text{NH}_3$  columns and  $\text{NH}_3$  profiles from MOZART-4 and validated it with forty four sites of Chinese Nationwide Nitrogen Deposition Monitoring Network (NNDMN). In one of the recent study over South Asia, interannual variability of atmospheric  $\text{NH}_3$  using IASI observations revealed large seasonal variability in atmospheric  $\text{NH}_3$  concentrations which were equivalent with highest number of urea fertilizer plants. This study highlights the importance of role of agriculture statistics and fertilizer consumption/application in determining ammonia concentration in South Asia

(Kuttippurath et al., 2020). Available global ammonia emission inventory does not include a comprehensive bottom up  $\text{NH}_3$  emissions for South Asia compared to East Asia to be suitable for input to atmospheric models by taking into consideration actual statistical data of various  $\text{NH}_3$  sources such as livestock excreta, fertilizer application, agricultural soil, nitrogen-fixing plants, crop residue compost, biomass burning, urine from rural populations, chemical industry, waste disposal, traffic, etc which is currently missing (Behera et al., 2013; Huang et al., 2012; Janssens-Maenhout et al., 2015; Li et al., 2017; Zhang et al., 2010). Han et al. (2020) suggested that updated emission inventory as per the source activity is essential for south Asia to reduce the uncertainties simulated  $\text{NH}_3$  over this region. A recent study by Wang et al. (2020) examined the  $\text{NH}_3$  column observed over the IGP during summer using regional model driven with MIX emission inventory. The study suggested that large agriculture activity and high summer temperature contributes to high  $\text{NH}_3$  emission fluxes over IGP which leads to large total columns. Summer time increase in  $\text{NH}_3$  concentration at surface over certain sites in the IGP regions are also observed from the ground based monitoring network (Datta et al., 2012; Mandal et al., 2013; Saraswati et al., 2019; Sharma et al., 2012, 2014b).

In this study, we examined the spatio-temporal variability of atmospheric  $\text{NH}_3$  over Asia (South and East Asia) and focus on two hotspots regions of ammonia, the Indo-Gangetic Plain (IGP) and the North China Plain (NCP). The approach for this study is a combination of simulations using chemical transport modelling, satellite observations and *in-situ* ammonia measurements over South Asia (69 stations) and East Asia (32 stations). The analysis applies the Model for Ozone and Related chemical tracers (MOZART-4) driven by priori ammonia emissions based on Hemispheric Transport of Air Pollution version-2 (HTAP-v2) emission inventory. It applies HTAP-v2 data for emissions to produce estimated total columns of  $\text{NH}_3$  and aerosol species for the year 2010 over Asia. Model simulations were evaluated and compared with  $\text{NH}_3$  data from IASI (over South and East Asia) and selected ground-based observations (noted above). In addition to the regional comparison, we examine why certain emission hotspot regions in East Asia show lower  $\text{NH}_3$  total columns compared with similar hotspot regions in South Asia, when analyzed with both model and satellite observations.

## 2. Data and methodology

### 2.1 MOZART-4 model

The global chemical transport model MOZART-4 has been employed in this study to conduct a year-long (2010) simulation of **atmospheric trace gases and aerosols** over Asia using the updated HTAP-v2 emission inventory (Janssens-Maenhout et al., 2015). These simulations were earlier performed to meet the objectives of Task Force on Hemispheric Transport of Air Pollution, phase 2, multi-model experiments (Surendran et al., 2015; Surendran et al., 2016). The model domain covers entire globe at a horizontal grid resolution of  $1.9^\circ \times 2.5^\circ$  and 56 vertical levels from the surface upto 1hectopascal (hPa). The model has approximately 10 levels in the boundary layer (below 850 hPa). MOZART-4 takes into account surface emissions, convection, advection, boundary layer transport, photochemistry, and wet and dry deposition. The model simulations were driven by the input meteorological data set of  $1.9^\circ \times 2.5^\circ$  resolution from Modern Era Retrospective-analysis for Research (MERRA) and Applications of the Goddard Earth Observing System Data Assimilation System (GEOS-DAS). Model simulations were performed for the complete year of 2010 (1 January 2010 to 31 December 2010) and its outputs were saved every 6h (4 time steps each day) with a spin up time of six months (1 July 2009 to 31

December 2009). MOZART-4 includes 157 gas-phase reactions, 85 gas-phase species, 39 photolysis and 12 bulk aerosol compounds (Emmons et al., 2010). Dry deposition of gases and aerosols were calculated online according to the parameterization of Wesely (1989) and wet deposition of soluble gases were calculated as described by the method of Emmons et al. (2010). Land use cover (LUC) maps used in MOZART-4 are based on the Advanced Very High Resolution Radiometer (AVHRR) and Moderate Resolution Imaging Spectroradiometer (MODIS) data based on NCAR Community Land Model (CLM) (Oleson et al., 2010). MOZART-4 represents the land surface as a hierarchy of sub-grid types: glacier, lake, wetland, urban and vegetated land. The vegetated land is further divided into a mosaic of Plant Function Type (PFTs). These same maps are used for the dry deposition calculations (Emmons et al., 2010; Oleson et al., 2010; Lawrence and Chase, 2007). In MOZART-4 the tropospheric aerosol component is built on the extended work of Tie et al. (2001 and 2005). Online fast Tropospheric Ultraviolet Visible (FTUV) scheme, based on the TUV model (Tie et al., 2003) is used for the calculation of photolysis rates in MOZART-4. For long-lived species like CH<sub>4</sub> and H<sub>2</sub>, surface boundary conditions are constrained by observations from NOAA/ESRL/GMD (Dlugokencky et al., 2005, 2008; Novelli et al., 1999) and as per Intergovernmental Panel N<sub>2</sub>O concentrations are set to the value as described in Intergovernmental Panel on Climate Change 2000 report (IPCC, 2000). Biogenic emissions of isoprene and monoterpenes are calculated online using the Model of Emissions of Gases and Aerosols from Nature (MEGAN) (Guenther et al., 2006), using the implementation described by Pfister et al. (2008). Surface moisture flux and all relevant physical parameters are used to calculate water vapor (H<sub>2</sub>O) online. Biomass burning emissions of a wide range of gaseous components, including NH<sub>3</sub>, SO<sub>2</sub> and individual volatile organic compounds were provided from the Global Fire Emission Database (GFED-v3), determined by scaling the GFED CO<sub>2</sub> emissions by the emission factors provided on 1.9° × 2.5° grid resolution (Emmons et al., 2010). In MOZART-4 the ammonium nitrate distribution is determined from NH<sub>3</sub> emissions and the parameterization of gas/aerosol partitioning using equilibrium simplified aerosol model (EQSAM) by Metzger et al. (2002), which is a set of approximations to the equilibrium constant calculation (Seinfeld et al., 1998), based on the level of sulphate present. In Metzger et al. (2002) cations other than NH<sub>4</sub><sup>+</sup>, e.g., sodium (Na<sup>+</sup>), potassium (K<sup>+</sup>), calcium (Ca<sup>2+</sup>), and magnesium (Mg<sup>2+</sup>) as well as organic acids have been neglected for the gas-aerosol partitioning calculations. Metzger et al. (2006) found that the NH<sub>3</sub>/NH<sub>4</sub><sup>+</sup> (calculated by account for ammonium-sulfate-nitrate-sodium-chloride-water system (updated-EQSAM2 parameterization considering organic acids) was 15 % lower than that calculated from the parameterization similar to EQSAM. Ammonia has stronger affinity towards neutralization of sulphuric acid (H<sub>2</sub>SO<sub>4</sub>) than nitric acid (HNO<sub>3</sub>) whereas formation of ammonium chloride (NH<sub>4</sub>Cl(s) or (aq)) in atmosphere is unstable and can dissociate reversibly to NH<sub>3</sub> and HCL. These aerosols in both dry and aqueous phase evaporate faster than the corresponding ammonium nitrate (NH<sub>4</sub>NO<sub>3</sub>) aerosols (Seinfeld and Pandis, 2012). In current modelling setup NH<sub>3</sub>/NH<sub>4</sub><sup>+</sup> partitioning is mainly controlled by sulfate and subsequently by nitrate. Recent study (Acharja et al., 2020) based on analysis of water soluble inorganic chemical ions of PM<sub>1</sub>, PM<sub>2.5</sub> and atmospheric trace gases over IGP revealed that NH<sub>4</sub><sup>+</sup> was one of the dominant ions, collectively with Cl<sup>-</sup>, NO<sub>3</sub><sup>-</sup> and SO<sub>4</sub><sup>-</sup> constituted more than 95 % of the measured ionic mass in both PM<sub>1</sub> and PM<sub>2.5</sub>. Remaining ionic species (i.e., Na<sup>+</sup>, K<sup>+</sup>, Ca<sup>2+</sup> and Mg<sup>2+</sup>) formed constituted only about 3 % of the total measured ions. Although major mineral cations (i.e., Na<sup>+</sup>, K<sup>+</sup>, Ca<sup>2+</sup> and Mg<sup>2+</sup>) contribute actively in neutralization reaction, but their concentration in IGP was found to be very low. Also over NCP, mineral cations contributed less than 5 % in both PM<sub>1</sub> and PM<sub>2.5</sub> (Dao et al., 2014). Furthermore, recent study by

Xu et al. (2017) over East Asia revealed that  $\text{NH}_4^+$  was the predominant neutralizing cation with the highest neutralization factor (NF) (above 1), whereas  $\text{Na}^+$ ,  $\text{K}^+$ ,  $\text{Ca}^{2+}$  and  $\text{Mg}^{2+}$  contributed relatively low (below 0.2). Therefore, consideration of mineral cations and organic acids on the  $\text{NH}_3/\text{NH}_4^+$  partitioning might be limited and will not have significant impact on the results of this study.

## 2.2 Emission inventory (HTAP-v2)

The HTAP-v2 bottom-up database is used in this study as an input for anthropogenic emissions of  $\text{NH}_3$  for the year 2010 (Janssens-Maenhout et al., 2015). HTAP-v2 dataset is embedded with the activity data as per harmonized emission factors, international standards, and gridded emissions with global proxy data. It includes important point sources providing high spatial resolution and emission grid maps with global coverage. This dataset consists of monthly mean  $\text{NH}_3$  emission maps with  $0.1^\circ \times 0.1^\circ$  grid resolution for the year 2010. The HTAP-v2 dataset is compiled using various regional gridded emission inventories by Environmental Protection Agency (EPA) for USA and Environment Canada for Canada, European Monitoring Evaluation Programme (EMEP) and Netherlands Organisation for Applied Scientific Research for Europe, and Model Inter comparison Study in Asia (MICS Asia) for China, India and other Asian countries. The emissions Database for Global Atmospheric Research (EDGAR v4.3) is used for the rest of the world (mainly South-America, Africa, Russia and Oceania). The ‘MICS Asia’ dataset incorporated into the HTAP-v2 dataset includes an anthropogenic emission inventory developed in 2010 (Li et al., 2015), which incorporates several local emission inventories, including the Multi-resolution Emission Inventory for China (MEIC),  $\text{NH}_3$  emission inventory from Peking University (Huang et al., 2012) and Regional Emission inventory in Asia version 2.1 (REAS2.1) (Kurokawa et al., 2013) for areas where local emission data are not available. A detailed description on HTAP-v2 datasets can be found in Janssens-Maenhout et al. (2015).

For this study, we used emissions from five important sectors, such as, agricultural, residential (heating/cooling of buildings and equipment/lighting of buildings and waste treatment), energy (power industry), transport (ground transport) and industries (manufacturing, mining, metal, cement, chemical, solvent industry) for the year 2010. The aircraft and international shipping is not considered for  $\text{NH}_3$  emissions in the HTAP-v2 bottom-up database. These emissions also includes natural emissions such as soil from the Community Earth System Model (CESM), and biomass burning from the Global Fire Emission Database (GFED-v3) (Randerson et al., 2013). All these emissions are re-gridded to  $1.9^\circ \times 2.5^\circ$  to match the model resolution.

The spatial distribution of the total  $\text{NH}_3$  emissions over Asian region is shown in Fig. 1. It shows the highest emissions over both South and East Asia, especially over the IGP and NCP region (shown with black box in Fig. 1). Agricultural sector is the main contributor to  $\text{NH}_3$  emission, including management of manure and agricultural soils (application of nitrogen fertilizers, including animal waste). It also includes emissions from livestock, crop cultivation excluding emissions from agricultural waste burning and savannah burning (Janssens-Maenhout et al., 2015). Minor contributions from the residential sector are also observed for the Asian countries due to use of biomass combustion and coal burning which is also included in the emissions. Spatial proxies such as population density, road networks, and land use information have been used to allocate area of emission sources. For the REAS2 emission inventory over India, the agricultural sector follows spatial proxy of total population (Li et al., 2017). The use of this approach is expected to be the main source of spatial uncertainty in the estimated  $\text{NH}_3$  emissions to the extent that total human population is only approximately correlated with

spatial distribution of fertilizer use and livestock numbers. Seasonal variation of average  $\text{NH}_3$  emission over the IGP and NCP region for Anthropogenic (HTAP-v2), biomass burning (GFED-v3) and Soil emission (CESM) is shown in Fig. 2. Anthropogenic  $\text{NH}_3$  emissions do not show any strong seasonal variability over the IGP region however over the NCP region,  $\text{NH}_3$  emissions show strong seasonality with peak emissions between May-September months. It can be seen that the magnitude of peak emissions is two times more over the NCP region than IGP region. On the other hand, seasonality in biomass burning  $\text{NH}_3$  emissions is strong over the IGP region, which shows highest emissions in the spring season (MAM). Also, contribution of  $\text{NH}_3$  emissions from the IGP region is significantly higher compared to NCP region during peak burning season, but the magnitude of biomass burning emission is six times lower compared to the magnitude of anthropogenic emissions.

### 2.3 Satellite $\text{NH}_3$ observations

The  $\text{NH}_3$  total columns data used in study are derived from the IASI space-borne remote sensing instrument on board Metop-A, which was launched in 2006 in a polar sun-synchronous orbit. The IASI operates in the thermal infrared spectral range ( $645\text{--}2760\text{ cm}^{-1}$ ) with mean local solar overpass time of 9:30 am and 9:30 pm (Clerbaux et al., 2009). It covers the globe twice a day with each observation is composed of 4 pixels with a circular footprint of 12 Kilometer (km) diameter at nadir and elliptical at the end of the swath ( $20 \times 39\text{ km}$ ). IASI is a suitable tool for evaluation of regional and global models due to its relatively high spatial and temporal sampling and retrieval algorithms have been continuously improved (Whitburn et al., 2016). The  $\text{NH}_3$  total column retrievals show reasonable agreement with monthly averaged integrated ground-based measurements with FTIR column data (Van Damme et al., 2015a). IASI measurements are also found to be consistent with other  $\text{NH}_3$  satellite products (Clarisse et al., 2010; Someya et al., 2020; Viatte et al., 2020). In present study, we have used ANNI- $\text{NH}_3$ -v2.2R-I dataset for the year 2010 which relies on ERA-Interim ECMWF meteorological input data, along with surface temperature retrieved from a dedicated network (Van Damme et al., 2017). An improved retrieval scheme for IASI spectra relies on the calculation of a dimensionless “Hyperspectral Range Index,” which is successively converted to the total column and allow a better identification of weak point sources of atmospheric  $\text{NH}_3$  (Van Damme et al., 2017; Whitburn et al., 2016). More details about IASI satellite and  $\text{NH}_3$  data product is given in Clerbaux et al. (2009), Van Damme et al. (2017) and Whitburn et al. (2016). We have considered the daily  $\text{NH}_3$  cloud-free satellite total column data and compared with the modelled daily  $\text{NH}_3$  total column averaging paired observations across the months, seasons and year. We have used only morning overpasses at 9:30 am measurements, as the relative errors due to the lower thermal contrast are larger for the night-time measurements (9:30 pm overpass). For consistency with satellite retrievals, first the model output (11:30 LT) at each day close to satellite overpass time (9:30 LT) is interpolated in space to the location of valid satellite retrievals. Since IASI retrieval algorithm only provides total columns, in second step, we made unweighted average distribution of the daily paired data to obtain a monthly, seasonal and annual mean value of satellite and model total  $\text{NH}_3$  columns at each horizontal resolution of the model ( $1.9^\circ \times 2.5^\circ$ ).

### 2.4 Ground based observations

To evaluate model performance in South Asia, we used hourly  $\text{NH}_3$  measurements from the air quality monitoring station (AQMS) network operated by Central Pollution Control Board (CPCB) across India. CPCB follows a national program for sampling of ambient air quality as well as weather parameters measurements. An

automatic analyzer (continuous) method is adopted at each monitoring location.  $\text{NH}_3$  is measured by the chemiluminescence method as  $\text{NO}_x$  following oxidation of  $\text{NH}_3$  to  $\text{NO}_x$ . In this approach,  $\text{NH}_3$  is determined from the difference between  $\text{NO}_x$  concentration with and without inclusion of  $\text{NH}_3$  oxidation (CPCB, 2011). The quality assurance and control process followed for these air quality monitoring instruments is given in CPCB (2014, 2020). Surface observations of  $\text{NH}_3$  are taken from 69 different stations in South Asia. Most of the  $\text{NH}_3$  monitoring stations from India used in the current study are situated in the cities representing the urban environment. Sampling of ambient  $\text{NH}_3$  is done through a sampling inlet of 1 meter (m) above the roof top of container AQMS having height of 2.5 m (Technical specifications, 2019). The details of these monitoring locations are given in Table S1 (in the Supplement) and the geographical locations are shown in Fig. 3. Out of these stations thirty five locations in Delhi, six in Bangalore city, four in Hyderabad, and two in Jaipur city are averaged to get single value for the same geographical location and the remaining 22 locations are considered independently representing 26 respective cities. Hourly  $\text{NH}_3$  concentrations (in  $\mu\text{g m}^{-3}$ ) used in the study are for the duration of 2016 to 2019. The quality control and assurance method, followed by Central Pollution Control Board (CPCB) for these air quality monitoring stations, is given in the CPCB (2011 and 2020). The calibration procedures for  $\text{NH}_3$  analyzer conforms to United States Environmental Protection Agency (USEPA) methodologies and include daily calibration checks, biweekly precision checks and linearity checks every six weeks. All analyzers undergo full calibration every six weeks. For detail on calibration procedure refer to Technical Specifications for Continuous Real Time Ambient Air Quality Monitoring Analysers (2016) and CPCB (2020). Furthermore, we take the following steps to reassure the quality of  $\text{NH}_3$  observations from the CPCB network stations. For data quality, we rejected all the observations values below the lowest detection limit of the instrument ( $1 \mu\text{g m}^{-3}$ ) (Technical specifications for CAAQM station, 2019) because most of the sites are situated in the urban environment. For cities where more than one monitoring station is available, we rejected all the observations above  $250 \mu\text{g m}^{-3}$  at a given site if other sites in the network do not show values outside this range. This step aims to eliminate any short-term local influence that cannot be captured in the models and retain the regional-scale variability. Second, we removed single peaks characterized by a change of more than  $100 \mu\text{g m}^{-3}$  in just one hour for all the data in CPCB monitoring stations. This step filters random fluctuations in the observations. Third, we removed some very high  $\text{NH}_3$  values that appeared in the timeseries right after the missing values. For any given day, we removed the sites from the consideration that either experience instrument malfunction, or appear to be very heavily influenced by strong local sources. In order to verify the data quality of CBCB monitoring site, we have inter compared the  $\text{NH}_3$  measurement at CPCB monitoring station (R.K. Puram) in Delhi with the  $\text{NH}_3$  measurements at Indira Gandhi International (IGI) Airport taken during Winter Fog Experiment (WiFEX) (Ghude et al., 2017) using Measurement of Aerosols and Gases (MARGA) instrument during winter season of 2017-2018. More details on the  $\text{NH}_3$  measurements using MARGA is available with Acharja et al. (2020). Both sites were situated in the same area of Delhi (less than 1km). Our inter-comparison show that  $\text{NH}_3$  measured at CPCB monitoring station by chemiluminescence method are slightly (on an average  $9.8 \mu\text{g m}^{-3}$ ) on higher side than  $\text{NH}_3$  measured by ion chromatography (IC) using MARGA (Fig. S1 in the Supplement). The differences that were observed could partly be related to the different  $\text{NH}_3$  measurement techniques and partly to the locations of the two monitoring sites which were not place exactly at same location. Apparently, the difference of  $9.8 \mu\text{g m}^{-3}$  indicates that the  $\text{NH}_3$  measurements from the CPCB do not suffer from the calibration issue. However, rigorous validation is required in the future

with more data sets. Given the presence of relatively high NO<sub>x</sub> concentrations, especially at urban locations, it is recognized that the measurement of NH<sub>3</sub> by difference (i.e., between NO<sub>x</sub> and NO<sub>x</sub> plus oxidized NH<sub>3</sub>), is a potentially significant source of uncertainty. Future measurement inter-comparisons are planned (rescheduled from 2020 to 2021 because of COVID-19) to allow the chemiluminescence method as used in the Indian network to be compared with a range of other NH<sub>3</sub> measurement methods (A. Moring et. al, 2020; The Global Challenges Research Fund (GCRF) South Asia Nitrogen hub).

To further evaluate model performance over East Asia, we used monthly mean NH<sub>3</sub> measurements from the 32 stations of the Nationwide Nitrogen Deposition Monitoring Network (NNDMN) of China, operated by China Agricultural University. The details of these monitoring locations are given in Table S2 (in the Supplement) and the geographical locations are shown in Fig. 3. Monthly mean NH<sub>3</sub> concentrations (in µg m<sup>-3</sup>) used in the study are for the duration of 2010 to 2015. Ambient concentrations of gaseous NH<sub>3</sub> were measured using an active Denuder for Long-Term Atmospheric sampling (DELTA) system. More detail about the data product is given by Xu et al. (2019). To compare the model with observation, simulated NH<sub>3</sub> from the model are compared with the surface-based observations by using bi-linear interpolation of model output to the geographical location and elevation of the observational sites.

### 3. Results and Discussion

#### 3.1 Annual mean NH<sub>3</sub> total columns over South Asia

Yearly-averaged 2010 distribution of NH<sub>3</sub> total columns over Asia simulated by MOZART-4 model and also retrieved with IASI instrument are shown in Fig. 4a and 4b. The total NH<sub>3</sub> columns simulated by the model show high Tropospheric Vertical Column Densities (TVCDs) of about 0.5-7×10<sup>16</sup> molecules cm<sup>-2</sup> over IGP region of India compared to any other regions of Asia. This may reflect the larger range of NH<sub>3</sub> column values for the South Asian model domain, with both more polluted and cleaner conditions. These high TVCDs values coincide with the high fertilizer-N and livestock numbers, as scaled according to human population density in Fig. 1.

Spatial differences between model simulated data and satellite data for NH<sub>3</sub> total column distribution are shown in Fig. 4c. On a quantitative level, the MOZART-4 model is found to overestimates the NH<sub>3</sub> total column compared with IASI by 1-4×10<sup>16</sup> molecules cm<sup>-2</sup> over South Asia, especially over northeast India and Bangladesh. Conversely, the MOZART-4 model underestimates NH<sub>3</sub> in comparison with IASI over the arid region of north western India (state of Rajasthan adjacent to Pakistan) and centering on Pakistan. There are several possible reasons for the spatial differences shown in Fig. 4c, including: a) uncertainties in the mapped NH<sub>3</sub> emissions data (e.g., between Afghanistan, Bangladesh, India and Pakistan, due to different relationships between human population and livestock/fertilizer activities); b) uncertainties related to turbulent mixing and dispersion (this may affect both the simulations in MOZART-4 and the assumed vertical profiles for the IASI retrievals); and c) uncertainties related to precipitation scavenging of ammonia and ammonium, noting that the eastern part of the IGP is substantially wetter than the western part.

According to Fig. 1, the magnitude of NH<sub>3</sub> emissions over NCP is similar to IGP. By contrast, much smaller TVCDs of the NH<sub>3</sub> columns are estimated by MOZART-4 and IASI over NCP compared with IGP. The MOZART-4 and IASI estimates are found to be in close agreement, with slightly smaller values estimated by

MOZART-4. The possible reasons for the difference in  $\text{NH}_3$  concentrations in IGP and NCP are discussed in Sect. 3.4. The relationship between modelled and IASI retrieved  $\text{NH}_3$  total columns are further analysed in terms of scatter plots in Fig. 5a and 5b, over IGP region of South Asia ( $20^\circ\text{N}$ - $32^\circ\text{N}$ ,  $70^\circ\text{E}$ - $95^\circ\text{E}$ ) and NCP region of East Asia ( $30^\circ\text{N}$ - $40^\circ\text{N}$ ,  $110^\circ\text{E}$ - $120^\circ\text{E}$ ) (rectangular areas shown in Fig. 1). Correlation coefficients ( $r$ ) between model and satellite observed annual mean total columns over IGP and NCP are found to be 0.81 and 0.90 respectively for 2010. This indicates that spatial variability in simulated  $\text{NH}_3$  by the model and satellite observation is in closer agreement, both over IGP and NCP region. The Model simulated annual mean total  $\text{NH}_3$  columns gives larger values over IGP region (Normalised Mean Bias (NMB) = 38 %) as well as over entire South Asia (NMB = 44 %). Whereas over the NCP region (NMB = -35 %) and entire East Asia (NMB = -32 %), the model gives values which are smaller than IASI. Other statistical indicators are summarised in Table 1. Larger estimates of  $\text{NH}_3$  columns from an atmospheric Chemistry Transport Model (CTM) compared with IASI was also found in an earlier study for South Asia (Clarisse et al., 2009).

The overall higher value of the model simulated  $\text{NH}_3$  over South Asia compared with IASI could be due to the combination of the uncertainties in both approaches. This includes uncertainties in emissions from the HTAP-v2 datasets used for the model simulations, inaccurate modelling of the chemistry in MOZART-4, errors in dry and wet deposition schemes used in the model, and biases inherent to infrared satellite remote sensing. For IASI, firstly, only cloud-free satellite scenes are processed, which could result in missing partly some of the  $\text{NH}_3$  values during cloudy periods and biomass burning events. Secondly,  $\text{NH}_3$  vertical columns retrieved from the IASI observations are actually sampled around 9:30 local time while the MOZART-4 simulated model output close to overpass time (11:30 LTC) was used. Finally, the retrieval of  $\text{NH}_3$  from infrared satellites is sensitive to inaccuracies in the temperature profile, and biases in the IASI L2 temperature profiles can result in biases in the retrieved  $\text{NH}_3$  (Whitburn et al., 2016). The HTAP-v2 dataset use proxy values for agricultural activities (i.e., distributed by human population) instead of actual values for field fertilizer application and livestock excretion over the South Asia. This could also result in additional uncertainty of  $\text{NH}_3$  emissions from the agricultural activities. Further work is on-going to integrate  $\text{NH}_3$  emissions inventories for different countries in South Asia based on national datasets, which should allow the emissions related uncertainties to be reduced in future. Similarly, slight underestimation over East Asia might originates from the country specific emission inventory used for China (Huang et al., 2012) in MOSAIC HTAP-v2 emission inventory and the limitations discussed above. The application of any equilibrium models (EQMs) in global atmospheric studies is associated with considerable uncertainties. In MOZART-4 chemistry, the ammonium nitrate distribution is determined from  $\text{NH}_3$  emissions and the parameterization of gas/aerosol partitioning by Metzger et al. (2002), based on the level of sulphate present. The emission fluxes of  $\text{SO}_2$  and  $\text{NO}_x$  in HTAP-v2 data set also has large uncertainties over the IGP (Jena et al., 2015b; Wang et al., 2020), which can introduce additional uncertainty in  $\text{NH}_3/\text{NH}_4^+$  gas/aerosol partitioning. In MOZART-4 chemistry, uncertainty can be also associated in dry and wet deposition scheme which can result in overestimation (Emmons et al., 2010).

### 3.2 Seasonal variability of $\text{NH}_3$ total columns

Figure 6 shows the model (left) and IASI satellite (middle) seasonal distributions of  $\text{NH}_3$  total columns over Asia. These seasons are represented as 3-month periods: Winter, December-January-February (DJF, first row), Spring, March-April-May (MAM, second row), Summer, June-July-August (JJA, third row), and Autumn,

September-October-November (SON, fourth row). It can be seen in Fig. 6, that there is larger seasonal variation in IASI NH<sub>3</sub> total columns while MOZART-4 presents limited seasonality as in South Asia compare to better seasonal variation estimated in East Asia, as shown by both IASI and the MOZART-4 model. In general, during autumn, spring, summer and winter seasons MOZART-4 shows higher NH<sub>3</sub> total column compared with IASI estimates over most of South Asia. However, this difference is more pronounced during autumn (SON) and winter (DJF) seasons (Fig. 6; Right). We have seen that (Fig. 2) anthropogenic emission of NH<sub>3</sub> is nearly same in all months and biomass burning has peak during MAM over South Asia in the MOZART-4 model. Whereas, seasonality is better represented in NH<sub>3</sub> emission for East Asia.

Major drivers in anthropogenic NH<sub>3</sub> seasonal variation include differences in management and timing of fertilizer, which is not well represented in the emission over South Asia (Janssens-Maenhout et al., 2012). This can be expected to have the direct effect on NH<sub>3</sub> total column over South Asia. It is recognized that NH<sub>3</sub> emission can be strongly affected by both short term meteorological variation and longer term climatic differences (Sutton et al., 2013). This means that NH<sub>3</sub> emissions may be expected to increase in warm summer conditions than in winter (Batty and Barrows, 2004). However, magnitude of these emissions is expected to be smaller in comparison with anthropogenic emissions and may not contribute significantly to larger summer time NH<sub>3</sub> columns observed from IASI retrievals over South Asia and East Asia than MOZART-4. Additional driver in NH<sub>3</sub> seasonal variation include meteorological variation. For example, strong subsidence, lower temperature and lighter winds over South Asia in the autumn and winter months prevent venting of low altitude pollution to the higher altitudes. This means that emitted air pollutants tend to accumulate close to the source region in winter time conditions (Ghude et al., 2010, 2011). Considering the comparison of IGP with NCP, accumulation of pollutants in the boundary layer is more pronounced over IGP region due to flat land topography, and it is more during winter than the autumn months (Surendran et al., 2016). We saw that simulated mean Planetary boundary layer height (PBLH) is lower (approximately 400 m, Fig. S2 in the Supplement), and winds are lighter in winter months, compared to summer months, over South Asia, and particularly over IGP region (Surendran et al., 2016). Figure 7 (left) and 7 (right) shows the time-height distribution of NH<sub>3</sub> and mean PBLH averaged over the IGP region, respectively. It can be seen that during winter months higher atmospheric stability prevents mixing of boundary layer NH<sub>3</sub> to the free troposphere over IGP (Fig. 7 (left)), which is reflected in the higher wintertime values of MOZART-4 NH<sub>3</sub> columns. Similarly, higher NH<sub>3</sub>/NH<sub>4</sub> ratio (Fig. S3 in the Supplement) and lower dry and wet deposition (Fig. S4 and S5 in the Supplement) of NH<sub>3</sub> over IGP in winter month enhances the accumulation of NH<sub>3</sub> in the boundary layer compared to summer months. On the other hand, very less NH<sub>3</sub> gets detected by the satellite at the higher altitudes where detection sensitivity of the satellite is more than that at the surface (Clarisse et al., 2010). Limited sensitivity of IASI measurements to detect boundary layer NH<sub>3</sub> (Van Damme et al., 2014a) could be one of the reasons for large differences ( $1-4 \times 10^{16}$  molecules cm<sup>-2</sup>) between MOZART-4 and IASI in winter seasons. Also, sowing of wheat crop over IGP involves higher rate of fertilizer application during peak winter month (Sharma et al., 2014) that release significant quantity of NH<sub>3</sub> into the atmosphere. However, this seasonality is largely missing in the emissions (Fig. 2 (top, left)) indicating that higher MOZART-4 NH<sub>3</sub> is largely driven by the winter-time meteorology over this region.

It is interesting to note from Fig. 6 (right) that during spring the difference between modelled and observed column NH<sub>3</sub> is smaller over the IGP region compared with the winter season. Heating of the landmass due to large solar incidence suppresses the wintertime subsidence over the IGP and leads to deeper boundary layer

during spring and early summer. It can be seen that (Fig. 7 (right) and Fig. S2 in the Supplement) the average PBLH is about 1100 m and 600 m deeper during spring and summer compared to winter over IGP. During this season, significant transport of the boundary pollution in the mid and upper troposphere due to enhanced convective activities and large scale vertical motion can be noticed in Fig. 7 (left) and is consistent with the earlier studies over this region (Lal et al., 2014; Surendran et al., 2016). Vertical motion associated with the convective activities is expected to redistribute the  $\text{NH}_3$  concentration in the column, which leads to more  $\text{NH}_3$  at the higher altitudes where detection sensitivity of the satellite is more than that at the surface (Clarisse et al., 2010). As a result, more  $\text{NH}_3$  gets detected by the satellite and we see less difference between observations and model over the IGP. This may also partly explain the higher IASI estimates of  $\text{NH}_3$  column for summertime prior to the monsoon season. However, this hypothesis needs to be tested with higher sensitivity experiments as a part of future work. During spring season, MOZART-4 reflects widespread  $\text{NH}_3$  total column from the entire Indian land mass and IASI observations does capture increase in  $\text{NH}_3$  total column at least for seasonal mean cycle (Fig. 8a). This seasonal maximum in  $\text{NH}_3$  total column identified both in IASI and MOZART-4 over South Asia can be explained by the two factors: Meteorology factor and biomass burning emissions. Volatilization of  $\text{NH}_3$  enhances with increase in temperature (Sutton et al., 2013), hence higher temperature during this drier periods over IGP partly enhances  $\text{NH}_3$  emission to the environment which is also evident from the soil  $\text{NH}_3$  emissions in Fig. 2 (bottom). However, magnitude of these emissions is expected to be smaller in comparison with anthropogenic emissions. In the Indian region, emissions from the biomass burning (crop-residue burning) peaks in March to May (Jena et al., 2015a) and emission of  $\text{NH}_3$  from biomass burning is maximum during this period (Fig. 2 (middle)). However, MOZART-4 estimates smaller  $\text{NH}_3$  total columns compared with IASI over Myanmar, Laos and Thailand during the period March-May (Fig. 6 (right)). This period is estimated to be associated with large scale forest fires (and open crop burning) (Chan, 2017; Wu et al., 2018; Zheng et al., 2017), the effect of which appears to be underestimated in the MOZART-4 simulations. It suggests that the Global Fire Emissions Database (GFED-v3) used in this study is low over this region agreeing with Zhang et al. (2020) and Huang et al. (2013). During the monsoon season (JJA) (Fig. 6 (right)) and summer, IASI- $\text{NH}_3$  total columns are larger than the MOZART-4 estimates over north-western arid region of South Asia, where monsoon rainfall is lowest (less than 30 cm). On the other hand,  $\text{NH}_3$  columns estimated by IASI are lower in the North-western IGP than the MOZART-4 simulations.

Figure 8 shows the comparison between IASI and modelled monthly time series of  $\text{NH}_3$  total columns over IGP ( $20^\circ\text{N}$ - $32^\circ\text{N}$ ,  $70^\circ\text{E}$ - $95^\circ\text{E}$ ) and NCP ( $30^\circ\text{N}$ - $40^\circ\text{N}$ ,  $110^\circ\text{E}$ - $120^\circ\text{E}$ ), respectively (rectangular areas shown on Fig. 1). We found a better consistency between modelled and measured seasonal  $\text{NH}_3$  total column over NCP than IGP. Monthly  $\text{NH}_3$  columns over the IGP show bimodal distribution in the model. However, IASI does not show such bimodal variation. Seasonal statistics show large normalised mean bias (38 %) and poor correlation ( $r=0.41$ ) between model and IASI. The bimodal distribution in  $\text{NH}_3$  total columns is partly driven by the biomass burning emissions, which show major peak in spring and another small peak in autumn (Fig. 2 (middle)), and partly by the meteorology as discussed in the previous section. During monsoon months (JJA), when South Asia receives significant rainfall all over, model simulations present lower  $\text{NH}_3$  total column, which is not seen in the IASI observations and also in the surface observations (Fig. 8a and 9b) over IGP. The reason for this discrepancy may be related with the flat  $\text{NH}_3$  emission over South Asia (Fig. 2). Usually large amount of fertilization application is expected during the warm month of June and July in the IGP which is not represented

in the HTAP-v2 emissions and therefore lower values in the model during monsoon month is mostly driven by the model meteorology. Lower values observed during monsoon season in general are attributed to increase wet scavenging of  $\text{NH}_3$  due to monsoon rain (Fig. S5 (left) in the Supplement) and influx of cleaner marine air from the Bay of Bengal and Arabian Sea through south-easterly and south-westerly wind (Ghude et al., 2008). On the other hand, monthly variation in IASI  $\text{NH}_3$  total columns over East Asia is found to be captured well by the model (Fig. 8b) and seems to follow the variation observed in the anthropogenic  $\text{NH}_3$  emission (Fig. 2), except for the month of July where IASI estimates substantially higher  $\text{NH}_3$  total columns than the model. The reason for this peak in the IASI data for July may be related to urea fertilizer application in warm July conditions (see temporal course of Enhanced Vegetation Index (Li et al., 2014)), which seems to be not represented well in the HTAP-v2 emissions. The overall statistics show slight good correlation ( $r=0.61$ ) between observed and simulated  $\text{NH}_3$  columns and negative normalised mean bias (NMB = -41 %).

### 3.3 Comparison between surface $\text{NH}_3$ measurements and simulated $\text{NH}_3$ concentrations in South and East Asia

To evaluate modelled surface  $\text{NH}_3$  concentrations in South Asia, we have used  $\text{NH}_3$  surface measurements from 69 monitoring locations over India for the years from 2016 to 2019. As 2010 data was not available, we make the hypothesis that measurement from 2016-2019 can be considered as representative from what have been measured in 2010. Out of these stations thirty five locations in Delhi, six in Bangalore city, four in Hyderabad, and two in Jaipur city are averaged to get single value for the same geographical location and the remaining 22 locations are considered independently representing 26 respective cities. Due to the lack of ground-based measurements performed in 2010, the following comparison will mainly be qualitative, although it is estimated that the main spatial features of Indian agriculture and  $\text{NH}_3$  emissions will be consistent between 2010 and 2016-2019. As per the RCP 8.5 (Kumar et al., 2018)  $\text{NH}_3$  emission from South Asia is expected to increase by less than 20 % from 2010 to 2020. Assuming a linear relationship between emission and surface concentration, it is expected that  $\text{NH}_3$  concentrations could be higher by about 10-15 % in 2016 to 2019.

It is interesting to note that the correlation between annual and monthly mean MOZART-4 simulated and measured  $\text{NH}_3$  concentration ( $r=0.82$  and  $r=0.62$ ) is better than the comparison between MOZART-4 and IASI for South Asia (Fig. 9). However, the MOZART-4 has systematically smaller estimated  $\text{NH}_3$  concentrations compared with the ground based measurement network (NMB = -47 %). It should be noted that most of the monitoring stations are situated in urban regions(cities) of India and therefore represents the urban environment, which may have locally higher  $\text{NH}_3$  concentrations due to traffic and human activities (Sharma et al., 2014). Since the MOZART-4 model is run relatively at coarse ( $1.9^\circ \times 2.5^\circ$ ) grid resolution the emissions may not capture the true variability in emissions at city scale. These surface  $\text{NH}_3$  sites are influenced by local emissions that are therefore not resolved by the MOZART-4 model. Therefore, when comparing coarse-scale models to observations, the model may have difficulties in resolving local scales effects (Surendran et al., 2015). Until the planned further evaluation of the chemiluminescence monitoring method for ammonia (measured by difference with  $\text{NO}_x$ ) is evaluated (as noted in Sect. 2.4), it is not possible to be certain the extent to which possible uncertainties in the measurement method contribute to the differences shown in Fig. 9b. While noting these uncertainties, it is worth noting that the ground based  $\text{NH}_3$  observation network confirms the occurrence of higher ground-level  $\text{NH}_3$  concentrations in autumn and winter, as simulated using MOZART-4 using the HTAP-v2 emissions inventory (Fig. 9b).

Comparison of Fig. 8a and 9b shows that the time course of ground level  $\text{NH}_3$  concentrations (as estimated by MOZART-4) is significantly different to the time course of total  $\text{NH}_3$  column (as also estimated by MOZART-4). Whereas the total column is largest in the summer (reflective of deeper atmospheric mixing and recirculation), and the ground level concentrations are largest during winter. Although it is not easy to use the IASI data to infer ground level  $\text{NH}_3$  concentrations, the stronger summer maximum of IASI (Fig. 8a) compared with MOZART-4, suggests that IASI would be in less close agreement with the ground based measurement network than MOZART-4 (Fig. 9b). While recognizing uncertainties in this interpretation, the key point is that large  $\text{NH}_3$  columns estimated by IASI for May-July are not reflected in the ground-based  $\text{NH}_3$  measurements from the Indian monitoring network.

Figure 10 shows the comparison between monthly mean (from 2010 to 2015 observations)  $\text{NH}_3$  surface measurements from 32 monitoring locations over China and modelled surface  $\text{NH}_3$  concentrations from the same location over East. Similar to South Asia the MOZART-4 has systematically smaller estimated  $\text{NH}_3$  concentrations compared with the ground based measurement network (NMB = -44 %) over East Asia. Figure 10b shows maximum  $\text{NH}_3$  concentration occurred in summer (JJA) denotes agreement with IASI measurements. Other statistical indicators are summarised in Table 2. Furthermore, high  $\text{NH}_3$  concentration from ground based measurements during JJA is consistent with the higher HTAP-v2 emissions (Fig. 2) (Huang et al., 2012) and higher  $\text{NH}_4\text{NO}_3$  concentration (Fig. S6 in the Supplement). Higher concentration of  $\text{NH}_4\text{NO}_3$  and can also lead to higher  $\text{NH}_3$  concentrations especially during summer due to its semi-volatile and unstable character at higher temperatures, as it is observed in East Asia. This implies that the  $\text{NH}_3$  emissions may play a vital role in determining the seasonal pattern of the ground  $\text{NH}_3$  concentrations. Summer peak may originate from fertilizer application, livestock emissions and volatilization of  $\text{NH}_3$  which is enhanced in higher temperature (Liu et al., 2017a).

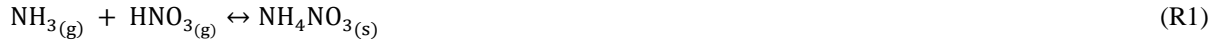
### 3.4 Why were $\text{NH}_3$ total columns low over high $\text{NH}_3$ emission over East Asia compared to high $\text{NH}_3$ emission region of South Asia?

Fine-scale details of the  $\text{NH}_3$  emissions over Asia in Fig. 1 and 2 clearly revealed larger emission values in areas where there is intensive agricultural management. This is the case especially in the NCP and IGP (Fig. 1, shown with box). Earlier emission estimates suggest that fertilizer application and livestock contribute 2.6 Tg per year ( $\text{yr}^{-1}$ ) and 1.7 Tg  $\text{yr}^{-1}$   $\text{NH}_3$  emissions respectively from South Asia (Aneja et al., 2011). Over South Asia, urea accounts for emissions of 2.5 Tg  $\text{yr}^{-1}$  which contributes to 95 % of the fertilizer emission, and 58 % of total estimated agricultural emissions (Fertilizer Association of India annual report 2018-19). For East Asia, livestock manure management accounts for approximately 54 % (5.3 Tg  $\text{yr}^{-1}$ ) of the total emissions and fertilizer application accounts for 33 % (3.2 Tg  $\text{yr}^{-1}$ ) emissions, with 13 % of emissions from other sources. Combined the model areas for NCP and IGP (as shown in Fig. 1) accounts for ~45 % of the  $\text{NH}_3$  emitted from fertilization in East Asia and South Asia (Huang et al., 2012).

We find that satellite observations show larger  $\text{NH}_3$  columns over IGP than over similar higher emission regions of NCP. However, in addition, we also find that the MOZART-4 model is able to capture this contrasting columnar  $\text{NH}_3$  levels between IGP and NCP. This indicates that the difference between IGP and NCP is unrelated to differences between the mosaic of emissions over South Asia and East Asia in HTAP-v2 and similarly not related to uncertainties in satellite retrievals. Instead, the analysis from MOZART-4 demonstrates that the difference can be explained by differences in atmospheric chemistry between the two regions, linked to

higher SO<sub>2</sub> and NO<sub>x</sub> emissions in the NCP than in the IGP. Recent study by Wang et al. (2020), shows that emission fluxes of SO<sub>2</sub> and NO<sub>x</sub> over IGP are only one-fourth of that over NCP.

As ammonia is a highly alkaline gas with an atmospheric lifetime usually of few hours (and rarely a few days) (Dammers et al., 2019), it readily reacts with acid present in the atmosphere to form aerosols, which are eventually deposited to the earth's surface by either dry or wet deposition processes (Fig. S4 and S5 in the Supplement). In the atmosphere, ammonia therefore reacts rapidly with atmospheric sulphuric acid (H<sub>2</sub>SO<sub>4</sub>), nitric acids (HNO<sub>3</sub>) and hydrochloric acid (HCl) to contribute to ambient levels of fine particles, forming ammonium sulphate, ammonium nitrate and ammonium chloride. Following reaction (R1) and (R2)



In the atmosphere, ammonium ion (NH<sub>4</sub><sup>+</sup>) as an aerosol is estimated to have a lifetime of about 1–15 days (Aneja et al., 1998), though this is obviously dependent on the amount of atmospheric acids (Seinfeld and Pandis, 2012). In addition to the large fertilizer application and livestock management activities which are characteristic of both IGP and NCP, industrial and transportation activities are higher over the NCP (China) which also results in higher emission of NO<sub>x</sub> and SO<sub>2</sub> over NCP compared with IGP (Zhao et al., 2013). Ammonia has greater affinity towards oxides of sulphur, hence it first reacts to form ammonium sulphate, and then the remaining ammonia further reacts to form ammonium nitrate (Seinfeld et al., 1998). The differences in the secondary aerosol formation over NCP and IGP are compared by considering the MOZART-4 model estimates of volume mixing ratio (VMR) in parts per billion (×10<sup>9</sup> ppb) of total sulphate, ammonium, ammonium nitrate at surface and total column of NO<sub>x</sub> (Fig. 11). Although vertical profiles of the aerosol components are small, there are strong vertical gradients in NO<sub>x</sub> concentrations, and for this reason we consider the comparison with the total NO<sub>x</sub> column more reflective of overall NO<sub>x</sub> chemistry than the ground level NO<sub>x</sub> VMR.

Figure 11 shows that total sulphate VMR (Fig. 11a) and NO<sub>x</sub> total column (Fig. 11c) are significantly higher over NCP region than IGP. Similarly, total ammonium VMR (Fig. 11b) is significantly larger over NCP than IGP indicating how a higher fraction of the gaseous ammonia is transformed to form ammonium over NCP region. In addition, Fig. 11d shows higher estimated levels of ammonium nitrate in MOZART-4 over NCP, reflective of the higher NO<sub>x</sub> emissions in this region. As a consequence of the different SO<sub>2</sub> and NO<sub>x</sub> sources, gaseous NH<sub>3</sub> is more quickly removed from atmosphere over East Asia with residence time of approximately 6 hours (Fig. S7 in the Supplement) (higher values indicates lower mean residence time), which is reflected in the higher VMR of ammonium, sulphate and ammonium nitrate (Fig. 11a, b and d). It can be seen that NH<sub>3</sub>/NH<sub>4</sub><sup>+</sup> ratio denotes lower values 0-1 (Fig. S3 in the Supplement) over East Asia than South Asia suggesting NH<sub>4</sub><sup>+</sup> partitioning is more over East Asia. As a result the NH<sub>3</sub> total columns over NCP are much smaller than over IGP, even though magnitude of NH<sub>3</sub> emission fluxes is greater over NCP than IGP.

#### 4. Conclusion

In this work, we have compared  $\text{NH}_3$  total columns simulated by the MOZART-4 model with IASI  $\text{NH}_3$  satellite observations over South and East Asia. The annual mean distribution reveals a consistent spatial pattern between MOZART-4 and IASI, but MOZART-4 tends to show larger  $\text{NH}_3$  columns over South Asia than IASI, particularly over the Indo-Gangetic Plain (IGP), whereas it is in close agreement over East Asia (including the North China Plain, NCP), with the exception of a July peak seen in the IASI dataset, which may be related to specific timing of fertilizer-related  $\text{NH}_3$  emissions. Comparison for seasonally and monthly resolved IASI total column with the MOZART-4 simulations shows inconsistencies in spatial and temporal pattern over South Asia. This inconsistency is due to the uncertainties in emission estimate which doesn't include seasonality pattern in HTAP-v2 over South Asia, as well as uncertainties in the processing of the IASI data. Both the MOZART-4 results and IASI estimates involve assumptions that could considerably affect the comparison between total columns of  $\text{NH}_3$ .

Comparison with estimates from a ground based  $\text{NH}_3$  monitoring network for both South and East Asia, our results showed that MOZART-4 systematically gives smaller  $\text{NH}_3$  concentration estimates than the monitoring network. The  $\text{NH}_3$  measurement sites used in present study mostly represent urban locations and model may not be able to capture actual concentration at point location due to coarser grid resolution over India. In addition, further assessment is needed to demonstrate the reliability of the  $\text{NH}_3$  measurement technique used in the monitoring network, where  $\text{NH}_3$  is measured by difference with  $\text{NO}_x$  concentrations, which may be uncertain in urban areas with high  $\text{NO}_x$  concentrations.

Despite the high  $\text{NH}_3$  emission over both South and East Asia, a larger  $\text{NH}_3$  total column is observed over South Asia in both the IASI and MOZART-4 estimates. This difference is explained by the MOZART-4 simulation, which treat the full atmospheric chemistry interaction with  $\text{SO}_2$  and  $\text{NO}_x$  emissions, leading to aerosol formation. The MOZART-4 model showed higher sulphate volume mixing ratio and  $\text{NO}_x$  total column over East Asia, especially in the NCP, which is reflected in ammonium aerosol volume mixing ratio (VMR) over East Asia. This suggests that the formation of ammonium aerosols (dominated by ammonium, sulphate and ammonium nitrate) is quicker over East Asia than in South Asia, leading to lower  $\text{NH}_3$  total columns in East Asia.

To examine the present findings future studies should investigate the effect of changing emissions of  $\text{NO}_x$  and  $\text{SO}_2$  on  $\text{NH}_3$  columns, for example by using perturbation of these emissions through counterfactual modeling scenarios. The comparison between model simulations using MOZART-4, satellite derived estimates from IASI and ground-based monitoring of  $\text{NH}_3$  concentrations has highlighted the known uncertainties in emissions, satellite retrievals and measurements at point locations. In order to reduce the uncertainties in ammonia emission, it would be a key to create an  $\text{NH}_3$  emission inventory specifically over South Asia, which is now currently under development as part of the GCRF South Asian Nitrogen Hub. This includes work to improve the bottom-up  $\text{NH}_3$  emission inventory, taking into account primary agricultural statistics on fertilizer use and animal number distributions. There is also potential for top-down (inverse modelling) for  $\text{NH}_3$  and  $\text{NO}_x$  by taking inference from the model, satellite and ground-based evidence. Here it is essential to recognize the need for more ground-based observational sites to measure  $\text{NH}_3$  air concentrations in rural areas where agriculture activity is predominant. Such measurements at present are currently very few for South Asia. Coarser global

models fail to resolve the local-scale emissions, hence higher resolution regional models with advance chemistry are also needed to resolve the sources and chemical processes on urban and rural scales.

#### **Data availability**

The  $0.1^{\circ} \times 0.1^{\circ}$  emission grid maps can be downloaded from the EDGAR website on [https://edgar.jrc.ec.europa.eu/htap\\_v2/index.php?SECURE=\\_123](https://edgar.jrc.ec.europa.eu/htap_v2/index.php?SECURE=_123) per year per sector. The model data can be downloaded upon request from the AeroCom database (<http://www.htap.org/>, last accessed June 22, 2020) (TF HTAP, 2018). The model data is available at Prithvi (IITM) super-computer and can be provided upon request to corresponding author. The morning overpass  $\text{NH}_3$  total columns measured through IASI can be accessed from data center at <http://cds-espri.ipsl.upmc.fr/etherTypo/index.php?id=1700&L=1>. For India, ground based hourly  $\text{NH}_3$  measurements can be obtained from CPCB website on <https://app.cpcbcr.com/ccr>. For China, ground based monthly mean  $\text{NH}_3$  datasets can be downloaded from [https://figshare.com/articles/Data\\_Descriptor\\_Xu\\_et\\_al\\_20181211\\_Scientific\\_data\\_docx/7451357](https://figshare.com/articles/Data_Descriptor_Xu_et_al_20181211_Scientific_data_docx/7451357).

#### **Author contributions**

All authors contributed to the research; SDG designed the research; PVP conducted the research; PVP and SDG wrote the paper; CJ and DS performed the MOZART model simulations; AM and MAS formulated the research; MVD, LC and PFC performed the IASI experiments; SK, DML, XL, WU, JJ, and TKA contributed to writing.

#### **Competing interests**

The authors declare that they have no conflict of interest.

#### **Acknowledgments**

We wish to thank the National Centre for Atmospheric Research (NCAR), funded by the U.S. National Science Foundation and operated by the University Corporation for Atmospheric Research, for access to the MOZART-4. All model runs were carried out on a Prithvi IBM High Performance Computing system at the Indian Institute of Tropical Meteorology (IITM), Pune India. We thank the Director, IITM for providing all the essential facilities required to complete the work. We wish to acknowledge the availability of CPCB data from CPCB webportal (<https://app.cpcbcr.com/ccr>). Research at ULB has been supported by the Belgian State Federal Office for Scientific, Technical and Cultural Affairs (Prodex arrangement IASI.FLOW). L.C. and M.V.D are respectively research associate and postdoctoral researcher with the Belgian F.R.S-FNRS. Cooperation between IITM and CEH has been facilitated through the NEWS India-UK Virtual Joint Centre, supported at CEH by the Biotechnological and Biological Sciences Research Council, and the Natural Environment Research Council of UK Research and Innovation (UKRI), and through the UKRI Global Challenges Research Fund (GCRF) South Asian Nitrogen Hub. The Nationwide Nitrogen Deposition Monitoring Network (NNDMN) of China was

619 supported by the Chinese National Natural Science Foundation (41425007) and the Chinese National Research  
620 Program for Key Issues in Air Pollution Control (DQGG0208).

## 621 **Financial support**

622 This research has been supported by “Urban modeling C-DAC” sponsored project.

## 623 **References**

624 A. Moring et. al: Nitrogen challenges and opportunities for agricultural and environmental science in India,  
625 Frontiers (Boulder)., doi:10.3389/fsufs.2021.505347, 2020.

626 Acharja, P., Ali, K., Trivedi, D. K., Safai, P. D., Ghude, S., Prabhakaran, T. and Rajeevan, M.: Characterization  
627 of atmospheric trace gases and water soluble inorganic chemical ions of PM<sub>1</sub> and PM<sub>2.5</sub> at Indira Gandhi  
628 International Airport, New Delhi during 2017–18 winter, Sci. Total Environ., 729, 138800,  
629 doi:10.1016/j.scitotenv.2020.138800, 2020.

630 Alexandratos, N. and Bruinsma, J.: World Agriculture Towards 2030 / 2050 The 2012 Revision. Global  
631 Perspective Studies Team, FAO Agricultural Development Economics Division. ESA Working Paper No. 12-  
632 03, (12), 2012.

633 Aneja, V. P., Murray, G. C. and Southerland, J.: Atmospheric nitrogen compounds: Emissions, transport,  
634 transformation, deposition, and assessment, EM Air Waste Manag. Assoc. Mag. Environ. Manag., 22–25, 1998.

635 Aneja, V. P., Battye, W., Behera, S. N., Erisman, J. W., Schlesinger, W. H. and Sharma, M.: Reactive nitrogen  
636 emissions from crop and livestock farming in India, Atmos. Environ., 47, 92–103,  
637 doi:10.1016/j.atmosenv.2011.11.026, 2011.

638 Battye, W. and B. R.: Review of Ammonia Emission Modeling Techniques for Natural Landscapes and  
639 Fertilized Soils, Work Assign. No. 2-09, 27517(68), 2004.

640 Behera, S. N., Sharma, M., Aneja, V. P. and Balasubramanian, R.: Ammonia in the atmosphere: a review on  
641 emission sources, atmospheric chemistry and deposition on terrestrial bodies, Environ. Sci. Pollut. Res., 20(11),  
642 8092–8131, doi:10.1007/s11356-013-2051-9, 2013.

643 Chan, K. L.: Biomass burning sources and their contributions to the local air quality in Hong Kong, Sci. Total  
644 Environ., 596–597, 212–221, doi:10.1016/j.scitotenv.2017.04.091, 2017.

645 Clarisse, L., Clerbaux, C., Dentener, F., Hurtmans, D. and Coheur, P. F.: Global ammonia distribution derived  
646 from infrared satellite observations, Nat. Geosci., 2(7), 479–483, doi:10.1038/ngeo551, 2009.

647 Clarisse, L., Shephard, M. W., Dentener, F., Hurtmans, D., Cady-Pereira, K., Karagulian, F., Van Damme, M.,  
648 Clerbaux, C. and Coheur, P. F.: Satellite monitoring of ammonia: A case study of the San Joaquin Valley, J.  
649 Geophys. Res. Atmos., 115(13), 1–15, doi:10.1029/2009JD013291, 2010.

650 Clarisse, L., Van Damme, M., Clerbaux, C. and Coheur, P. F.: Tracking down global NH<sub>3</sub> point sources with  
651 wind-adjusted superresolution, Atmos. Meas. Tech., 12(10), 5457–5473, doi:10.5194/amt-12-5457-2019, 2019.

652 Clerbaux, C., Boynard, A., Clarisse, L., George, M., Hadji-Lazaro, J., Herbin, H., Hurtmans, D., Pommier, M.,  
653 Razavi, A., Turquety, S., Wespes, C. and Coheur, P. F.: Monitoring of atmospheric composition using the  
654 thermal infrared IASI/MetOp sounder, Atmos. Chem. Phys., 9(16), 6041–6054, doi:10.5194/acp-9-6041-2009,  
655 2009.

656 CPCB: Guidelines for Real Time Sampling and Analyses., 2011.

657 CPCB: Annual Report 2014-15., 2014.

658 CPCB: Central Pollution Control Board (2020), [online] Available from: [https://cpcb.nic.in/quality-assurance-](https://cpcb.nic.in/quality-assurance-quality-control/)  
659 [quality-control/](https://cpcb.nic.in/quality-assurance-quality-control/).

660 Crippa, M., Guizzardi, D., Muntean, M., Schaaf, E., Dentener, F., Van Aardenne, J. A., Monni, S., Doering, U.,  
661 Olivier, J. G. J., Pagliari, V. and Janssens-Maenhout, G.: Gridded emissions of air pollutants for the period  
662 1970-2012 within EDGAR v4.3.2, *Earth Syst. Sci. Data*, 10(4), 1987–2013, doi:10.5194/essd-10-1987-2018,  
663 2018.

664 Van Damme, M., Whitburn, S., Clarisse, L., Clerbaux, C., Hurtmans, D. and Coheur, P.-F.: Version 2 of the  
665 IASI NH<sub>3</sub> neural network retrieval algorithm; near-real time and reanalysed datasets, *Atmos. Meas. Tech.*  
666 *Discuss.*, 1–14, doi:10.5194/amt-2017-239, 2017.

667 Van Damme, M., Clarisse, L., Whitburn, S., Hadji-Lazaro, J., Hurtmans, D., Clerbaux, C. and Coheur, P. F.:  
668 Industrial and agricultural ammonia point sources exposed, *Nature*, 564(7734), 99–103, doi:10.1038/s41586-  
669 018-0747-1, 2018.

670 Van Damme, Wichink Kruit, R. J., Schaap, M., Clarisse, L., Clerbaux, C., Coheur, P. F., Damers, E., Dolman,  
671 A. J. and Erisman, J. W.: Evaluating 4 years of atmospheric ammonia (NH<sub>3</sub>) over Europe using IASI satellite  
672 observations and LOTOS-EUROS model results, *J. Geophys. Res.*, 119(15), 9549–9566,  
673 doi:10.1002/2014JD021911, 2014a.

674 Van Damme, M., Hurtmans, D., Coheur, P. F., Clerbaux, C., Dolman, A. J., Erisman, J. W., Clarisse, L., Ngadi,  
675 Y. and Heald, C. L.: Global distributions, time series and error characterization of atmospheric ammonia (NH<sub>3</sub>)  
676 from IASI satellite observations, *Atmos. Chem. Phys.*, 14(6), 2905–2922, doi:10.5194/acp-14-2905-2014,  
677 2014b.

678 Van Damme, Damers, E., Flechard, C. R., Coheur, P. F., Xu, W., Erisman, J. W., Galy-Lacaux, C., Neuman,  
679 J. A., Clerbaux, C., Van Damme, M., Tang, Y. S., Liu, X., Sutton, M. A., Nowak, J. B. and Clarisse, L.: Towards  
680 validation of ammonia (NH<sub>3</sub>) measurements from the IASI satellite, *Atmos. Meas. Tech.*, 8(3), 1575–1591,  
681 doi:10.5194/amt-8-1575-2015, 2015a.

682 Van Damme, Erisman, J. W., Clarisse, L., Damers, E., Whitburn, S., Clerbaux, C., Dolman, A. J. and Coheur,  
683 P.: Worldwide spatiotemporal atmospheric ammonia (NH<sub>3</sub>), *Geophys. Res. Lett.*, 1–9,  
684 doi:10.1002/2015GL065496, 2015b.

685 Damers, E., McLinden, C. A., Griffin, D., Shephard, M. W., Van Der Graaf, S., Lutsch, E., Schaap, M.,  
686 Gainairu-Matz, Y., Fioletov, V., Van Damme, M., Whitburn, S., Clarisse, L., Cady-Pereira, K., Clerbaux, C.,  
687 Francois Coheur, P. and Erisman, J. W.: NH<sub>3</sub> emissions from large point sources derived from CrIS and IASI  
688 satellite observations, *Atmos. Chem. Phys.*, 19(19), 12261–12293, doi:10.5194/acp-19-12261-2019, 2019.

689 Dao, X., Wang, Z., Lv, Y., Teng, E., Zhang, L. and Wang, C.: Chemical characteristics of water-soluble ions in  
690 particulate matter in three metropolitan areas in the North China Plain, *PLoS One*, 9(12), 1–16,  
691 doi:10.1371/journal.pone.0113831, 2014.

692 Datta, A., Sharma, S. K., Harit, R. C., Kumar, V., Mandal, T. K. and Pathak, H.: Ammonia emission from  
693 subtropical crop land area in India, *Asia-Pacific J. Atmos. Sci.*, 48(3), 275–281, doi:10.1007/s13143-012-0027-  
694 1, 2012.

695 Dlugokencky, E. J., Myers, R. C., Lang, P. M., Masarie, K. A., Crotwell, A. M., Thoning, K. W., Hall, B. D.,  
696 Elkins, J. W. and Steele, L. P.: Conversion of NOAA atmospheric dry air CH<sub>4</sub> mole fractions to a  
697 gravimetrically prepared standard scale, *J. Geophys. Res. D Atmos.*, 110(18), 1–8, doi:10.1029/2005JD006035,  
698 2005.

699 Emmons, L. K., Walters, S., Hess, P. G., Lamarque, J. F., Pfister, G. G., Fillmore, D., Granier, C., Guenther, A.,  
700 Kinnison, D., Laepple, T., Orlando, J., Tie, X., Tyndall, G., Wiedinmyer, C., Baughcum, S. L. and Kloster, S.:  
701 Description and evaluation of the Model for Ozone and Related chemical Tracers, version 4 (MOZART-4),  
702 *Geosci. Model Dev.*, 3(1), 43–67, doi:10.5194/gmd-3-43-2010, 2010.

703 Fertilizer Association of India annual report 2018-19: Fertilizer Association of India annual report 2018-19.,  
704 2018.

705 Ghude, S. D., Fadnavis, S., Beig, G., Polade, S. D. and van der A, R. J.: Detection of surface emission hot spots,  
706 trends, and seasonal cycle from satellite-retrieved NO<sub>2</sub> over India, *J. Geophys. Res.*, 113(D20), D20305,  
707 doi:10.1029/2007JD009615, 2008.

708 Ghude, S. D., Lal, D. M., Beig, G., van der A, R. and Sable, D.: Rain-Induced Soil NO<sub>x</sub> Emission From India  
709 During the Onset of the Summer Monsoon: A Satellite Perspective, *J. Geophys. Res.*, 115(D16), D16304,  
710 doi:10.1029/2009JD013367, 2010.

711 Ghude, S. D., Beig, G., Kulkarni, P. S., Kanawade, V. P., Fadnavis, S., Remedios, J. J. and Kulkarni, S. H.:  
712 Regional co pollution over the Indian-subcontinent and various transport pathways as observed by mopitt, *Int. J.*  
713 *Remote Sens.*, 32(21), 6133–6148, doi:10.1080/01431161.2010.507796, 2011.

714 Ghude, S. D., Kulkarni, S. H., Jena, C., Pfister, G. G., Beig, G., Fadnavis, S. and Van Der, R. J.: Application of  
715 satellite observations for identifying regions of dominant sources of nitrogen oxides over the indian  
716 subcontinent, *J. Geophys. Res. Atmos.*, 118(2), 1075–1089, doi:10.1029/2012JD017811, 2013.

717 Ghude, S. D., Chate, D. M., Jena, C., Beig, G., Kumar, R., Barth, M. C., Pfister, G. G., Fadnavis, S. and Pithani,  
718 P.: Premature mortality in India due to PM<sub>2.5</sub> and ozone exposure, *Geophys. Res. Lett.*, 43(9), 4650–4658,  
719 doi:10.1002/2016GL068949, 2016.

720 Ghude, S. D., Bhat, G. S., Prabhakaran, T., Jenamani, R. K., Chate, D. M., Safai, P. D., Karipot, A. K., Konwar,  
721 M., Pithani, P., Sinha, V., Rao, P. S. P., Dixit, S. A., Tiwari, S., Todekar, K., Varpe, S., Srivastava, A. K., Bisht,  
722 D. S., Murugavel, P., Ali, K., Mina, U., Dharua, M., Rao, Y. J., Padmakumari, B., Hazra, A., Nigam, N.,  
723 Shende, U., Lal, D. M., Chandra, B. P., Mishra, A. K., Kumar, A., Hakkim, H., Pawar, H., Acharja, P.,  
724 Kulkarni, R., Subharthi, C., Balaji, B., Varghese, M., Bera, S. and Rajeevan, M.: Winter fog experiment over the  
725 Indo-Gangetic plains of India, *Curr. Sci.*, 112(4), doi:10.18520/cs/v112/i04/767-784, 2017.

726 Guenther, A., Karl, T., Harley, P., Wiedinmyer, C., Palmer, P. I. and Geron, C.: Estimates of global terrestrial  
727 isoprene emissions using MEGAN (Model of Emissions of Gases and Aerosols from Nature), *Atmos. Chem.*  
728 *Phys.*, 6(11), 3181–3210, doi:10.5194/acp-6-3181-2006, 2006.

729 Han, X., Zhu, L., Liu, M., Song, Y. and Zhang, M.: Numerical analysis of the impact of agricultural emissions  
730 on PM<sub>2.5</sub> in China using a high-resolution ammonia emissions inventory, *Atmos. Chem. Phys.*, (March), 1–31,  
731 doi:10.5194/acp-2019-1128, 2020.

732 Huang, K., Fu, J. S., Hsu, N. C., Gao, Y., Dong, X., Tsay, S. C. and Lam, Y. F.: Impact assessment of biomass  
733 burning on air quality in Southeast and East Asia during BASE-ASIA, *Atmos. Environ.*, 78(2012), 291–302,  
734 doi:10.1016/j.atmosenv.2012.03.048, 2013.

735 Huang, X., Song, Y., Li, M., Li, J., Huo, Q., Cai, X., Zhu, T., Hu, M. and Zhang, H.: A high-resolution  
736 ammonia emission inventory in China, *Global Biogeochem. Cycles*, 26(1), 1–14, doi:10.1029/2011GB004161,  
737 2012.

738 Janssens-Maenhout G., Dentener F., Van Aardenne J., Monni S., Pagliari V., Orlandini L., Klimont Z.,  
739 Kurokawa J., Akimoto H., Ohara T., Wankmueller R., Battye B., Grano D., Zuber A., K. T. .: EDGAR-HTAP: a  
740 Harmonized Gridded Air Pollution Emission Dataset Based on National Inventories, Ispra (Italy): European  
741 Commission Publications Office, , (February), 1–18, doi:ISBN 978-92-79-23122-0, ISSN 1831-9424, 2012.

742 Janssens-Maenhout, G., Dentener, F. J., Aardenne, J. Van, Monni, S., Pagliari, V., Orlandini, L., Klimont, Z.,  
743 Kurokawa, J., Akimoto, H., Ohara, T., Wankmüller, R., Battye, B., Grano, D., Zuber, A. and Keating, T.:  
744 EDGAR-HTAP: a harmonized gridded air pollution emission dataset based on national inventories., 2012.

745 Janssens-Maenhout, G., Koffi, B., Crippa, M., Pouliot, G., Zhang, Q., Wankmüller, R., Frost, G., Dentener, F.,  
746 Li, M., Guizzardi, D., Denier van der Gon, H., Darras, S., Kuenen, J. J. P., Keating, T., Klimont, Z., Kurokawa,  
747 J. and Muntean, M.: HTAP\_v2.2: a mosaic of regional and global emission grid maps for 2008 and 2010 to  
748 study hemispheric transport of air pollution, *Atmos. Chem. Phys.*, 15(19), 11411–11432, doi:10.5194/acp-15-  
749 11411-2015, 2015.

750 Jena, C., Ghude, S. D., Pfister, G. G., Chate, D. M., Kumar, R., Beig, G., Surendran, D. E., Fadnavis, S. and Lal,  
751 D. M.: Influence of springtime biomass burning in South Asia on regional ozone (O<sub>3</sub>): A model based case

study, *Atmos. Environ.*, 100, 37–47, doi:10.1016/j.atmosenv.2014.10.027, 2015a.

Jena, C., Ghude, S. D., Beig, G., Chate, D. M., Kumar, R., Pfister, G. G., Lal, D. M., Surendran, D. E., Fadnavis, S. and van der A, R. J.: Inter-comparison of different NO<sub>x</sub> emission inventories and associated variation in simulated surface ozone in Indian region, *Atmos. Environ.*, 117, 61–73, doi:10.1016/j.atmosenv.2015.06.057, 2015b.

Kumar, R., Barth, M. C., Pfister, G. G., Delle Monache, L., Lamarque, J. F., Archer-Nicholls, S., Tilmes, S., Ghude, S. D., Wiedinmyer, C., Naja, M. and Walters, S.: How Will Air Quality Change in South Asia by 2050?, *J. Geophys. Res. Atmos.*, 123(3), 1840–1864, doi:10.1002/2017JD027357, 2018.

Kurokawa, J., Ohara, T., Morikawa, T., Hanayama, S., Janssens-Maenhout, G., Fukui, T., Kawashima, K. and Akimoto, H.: Emissions of air pollutants and greenhouse gases over Asian regions during 2000–2008: Regional Emission inventory in ASia (REAS) version 2, *Atmos. Chem. Phys.*, 13(21), 11019–11058, doi:10.5194/acp-13-11019-2013, 2013.

Kuttippurath, J., Singh, A., Dash, S. P., Mallick, N., Clerbaux, C., Van Damme, M., Clarisse, L., Coheur, P. F., Raj, S., Abhishek, K. and Varikoden, H.: Record high levels of atmospheric ammonia over India: Spatial and temporal analyses, *Sci. Total Environ.*, 740, 139986, doi:10.1016/j.scitotenv.2020.139986, 2020.

Lal, D. M., Ghude, S. D., Singh, J. and Tiwari, S.: Relationship between Size of Cloud Ice and Lightning in the Tropics, , doi:10.1155/2014/471864, 2014.

Lawrence, P. J. and Chase, T. N.: Representing a new MODIS consistent land surface in the Community Land Model (CLM 3.0), *J. Geophys. Res. Biogeosciences*, 112(1), doi:10.1029/2006JG000168, 2007.

Li, L., Friedl, M. A., Xin, Q., Gray, J., Pan, Y. and Frohling, S.: Mapping Crop Cycles in China Using MODIS-EVI Time Series, , (September), doi:10.3390/rs6032473, 2014.

Li, M., Zhang, Q., Kurokawa, J., Woo, J., He, K. B., Lu, Z. and Ohara, T.: MIX : a mosaic Asian anthropogenic emission inventory for the MICS-Asia and the HTAP projects, , 34813–34869, doi:10.5194/acpd-15-34813-2015, 2015.

Li, M., Zhang, Q., Kurokawa, J. I., Woo, J. H., He, K., Lu, Z., Ohara, T., Song, Y., Streets, D. G., Carmichael, G. R., Cheng, Y., Hong, C., Huo, H., Jiang, X., Kang, S., Liu, F., Su, H. and Zheng, B.: MIX: A mosaic Asian anthropogenic emission inventory under the international collaboration framework of the MICS-Asia and HTAP, *Atmos. Chem. Phys.*, 17(2), 935–963, doi:10.5194/acp-17-935-2017, 2017.

Liu, L., Zhang, X., Xu, W., Liu, X., Li, Y., Lu, X., Zhang, Y. and Zhang, W.: Temporal characteristics of atmospheric ammonia and nitrogen dioxide over China based on emission data, satellite observations and atmospheric transport modeling since 1980, *Atmos. Chem. Phys.*, 17(15), 9365–9378, doi:10.5194/acp-17-9365-2017, 2017a.

Liu, X., Xu, W., Duan, L., Du, E., Pan, Y., Lu, X., Zhang, L., Wu, Z., Wang, X., Zhang, Y., Shen, J., Song, L., Feng, Z., Liu, X., Song, W., Tang, A., Zhang, Y., Zhang, X. and Collett, J. L.: Atmospheric Nitrogen Emission, Deposition, and Air Quality Impacts in China: an Overview, *Curr. Pollut. Reports*, 3(2), 65–77, doi:10.1007/s40726-017-0053-9, 2017b.

Mandal, T. K., Saxena, M., Rohtash, Sharma, S. K., Gupta, N. C., Kumar, M. and Saraswati: Characteristics of ambient ammonia over Delhi, India, *Meteorol. Atmos. Phys.*, 124(1–2), 67–82, doi:10.1007/s00703-013-0299-8, 2013.

Metzger, S., Dentener, F., Pandis, S. and Lelieveld, J.: Gas/aerosol partitioning: 1. A computationally efficient model, *J. Geophys. Res. Atmos.*, 107(16), doi:10.1029/2001JD001102, 2002.

Metzger, S., Mihalopoulos, N. and Lelieveld, J.: Importance of mineral cations and organics in gas-aerosol partitioning of reactive nitrogen compounds: Case study based on MINOS results, *Atmos. Chem. Phys.*, 6(9), 2549–2567, doi:10.5194/acp-6-2549-2006, 2006.

Oleson, K. W., Lawrence, D. M., Bonan, G. B., Flanner, M. G., Kluzek, E., Lawrence, P. J., Zeng, X. (2010):.

797 Technical Description of version 4.0 of the Community Land Model (CLM)., 2010.

798 Pfister, G. G., Emmons, L. K., Hess, P. G., Lamarque, J. F., Orlando, J. J., Walters, S., Guenther, A., Palmer, P.  
799 I. and Lawrence, P. J.: Contribution of isoprene to chemical budgets: A model tracer study with the NCAR  
800 CTM MOZART-4, *J. Geophys. Res. Atmos.*, 113(5), doi:10.1029/2007JD008948, 2008.

801 Pinder, R. W., Adams, P. J. and Pandis, S. N.: Ammonia Emission Controls as a Cost-Effective Strategy for  
802 Reducing Atmospheric Particulate Matter in the Eastern United States, *Environ. Sci. Technol.*, 41(2), 380–386,  
803 doi:10.1021/es060379a, 2007.

804 Pinder, R. W., Gilliland, A. B. and Dennis, R. L.: Environmental impact of atmospheric NH<sub>3</sub> emissions under  
805 present and future conditions in the eastern United States, *Geophys. Res. Lett.*, 35(12),  
806 doi:10.1029/2008GL033732, 2008.

807 Pollution, C. and Board, C.: Guidelines for Manual Sampling and Analyses., 2011.

808 Randerson, J., Werf, G. Van Der, Giglio, L., DAAC, G. C.-O. and 2015, Global Fire Emissions Database,  
809 Version 4.1 (GFEDv4), daac.ornl.gov.

810 Saraswati, George, M. P., Sharma, S. K., Mandal, T. K. and Kotnala, R. K.: Simultaneous Measurements of  
811 Ambient NH<sub>3</sub> and Its Relationship with Other Trace Gases, PM<sub>2.5</sub> and Meteorological Parameters over Delhi,  
812 India, *Mapan - J. Metrol. Soc. India*, 34(1), 55–69, doi:10.1007/s12647-018-0286-0, 2019.

813 Seinfeld, J. H. and Pandis, S. N.: Atmospheric Chemistry and Physics: From Air Pollution to Climate Change,  
814 Wiley., 2012.

815 Seinfeld, J. H., Pandis, S. N. and Noone, K.: Atmospheric Chemistry and Physics: From Air Pollution to  
816 Climate Change, *Phys. Today*, 51(10), 88–90, doi:10.1063/1.882420, 1998.

817 Sharma, S. K., Saxena, M., Saud, T., Korpole, S. and Mandal, T. K.: Measurement of NH<sub>3</sub>, NO, NO<sub>2</sub> and related  
818 particulates at urban sites of indo gangetic plain (IGP) of India, *J. Sci. Ind. Res. (India)*, 71(5), 360–362, 2012.

819 Sharma, S. K., Harit, R. C., Kumar, V., Mandal, T. K. and Pathak, H.: Ammonia Emission from Rice-Wheat  
820 Cropping System in Subtropical Soil of India, *Agric. Res.*, 3(2), 175–180, doi:10.1007/s40003-014-0107-9,  
821 2014a.

822 Sharma, S. K., Kumar, M., Rohtash, Gupta, N. C., Saraswati, Saxena, M. and Mandal, T. K.: Characteristics of  
823 ambient ammonia over Delhi, India., 2014b.

824 Someya, Y., Imasu, R., Shiomi, K. and Saitoh, N.: Atmospheric ammonia retrieval from the TANSO-  
825 FTS/GOSAT thermal infrared sounder, *Atmos. Meas. Tech.*, 13(1), 309–321, doi:10.5194/amt-13-309-2020,  
826 2020.

827 Surendran, D., Jena, C., Beig, G., Chate, D. M. and Ghude, S. D.: Quantifying the sectoral contribution of  
828 pollution transport from South Asia during summer and winter monsoon seasons in support of HTAP-2  
829 experiment, *Atmos. Environ.*, 145, 60–71, doi:10.1016/j.atmosenv.2016.09.011, 2016.

830 Surendran, D. E., Ghude, S. D., Beig, G., Emmons, L. K., Jena, C., Kumar, R., Pfister, G. G. and Chate, D. M.:  
831 Air quality simulation over South Asia using Hemispheric Transport of Air Pollution version-2 (HTAP-v2)  
832 emission inventory and Model for Ozone and Related chemical Tracers (MOZART-4), *Atmos. Environ.*, 122,  
833 357–372, doi:10.1016/j.atmosenv.2015.08.023, 2015.

834 Sutton, M. A., Reis, S., Riddick, S. N., Dragosits, U., Nemitz, E., Theobald, M. R., Tang, Y. S., Braban, C. F.,  
835 Vieno, M., Dore, A. J., Mitchell, R. F., Wanless, S., Daunt, F., Fowler, D., Blackall, T. D., Milford, C.,  
836 Flechard, C. R., Loubet, B., Massad, R., Cellier, P., Personne, E., Coheur, P. F., Clarisse, L., Van Damme, M.,  
837 Ngadi, Y., Clerbaux, C., Skjøth, C. A., Geels, C., Hertel, O., Kruit, R. J. W., Pinder, R. W., Bash, J. O., Walker,  
838 J. T., Simpson, D., Horváth, L., Misselbrook, T. H., Bleeker, A., Dentener, F. and de Vries, W.: Towards a  
839 climate-dependent paradigm of ammonia emission and deposition, *Philos. Trans. R. Soc. B Biol. Sci.*,  
840 368(1621), 20130166–20130166, doi:10.1098/rstb.2013.0166, 2013.

841 Sutton, M. A., J. Drewer, A. Moring, T.K Adhya, A. Ahmed and A. Bhatia: The Indian nitrogen assessment :  
842 sources of reactive nitrogen, environmental and climate effects, management options, and policies, in The  
843 Indian Nitrogen Assessment, edited by Y. P. Abrol, T. K. Adhya, V. P. Aneja, N. Raghuram, H. Pathak, U.  
844 Kulshrestha, C. Sharma, and B. Singh, pp. 9–25, Elsevier., 2017.

845 Technical specifications for CAAQM station: Technical specifications for continuous ambient air quality  
846 monitoring (CAAQM) STATION (real time) Central Pollution Control Board East Arjun Nagar, Shahdara.,  
847 2019.

848 Technical Specifications for Continuous Real Time Ambient Air Quality Monitoring Analysers: Technical  
849 Specifications for Continuous Real Time Ambient Air Quality Monitoring Analysers / Station Volume – II.,  
850 2016.

851 The Global Challenges Research Fund (GCRF) South Asia Nitrogen hub: The Global Challenges Research  
852 Fund (GCRF) project, [online] Available from: <https://gtr.ukri.org/projects?ref=NE/S009019/1>.

853 Tie, X., Brasseur, G., Emmons, L., Horowitz, L. and Kinnison, D.: Effects of aerosols on tropospheric oxidants:  
854 A global model study, *J. Geophys. Res. Atmos.*, 106(D19), 22931–22964, doi:10.1029/2001JD900206, 2001.

855 Tie, X., Madronich, S., Walters, S., Zhang, R., Rasch, P. and Collins, W.: Effect of clouds on photolysis and  
856 oxidants in the troposphere, , 108, doi:10.1029/2003JD003659, 2003.

857 Tie, X., Madronich, S., Walters, S., Edwards, D. P., Ginoux, P., Mahowald, N., Zhang, R. Y., Lou, C. and  
858 Brasseur, G.: Assessment of the global impact of aerosols on tropospheric oxidants, *J. Geophys. Res. D Atmos.*,  
859 110(3), 1–32, doi:10.1029/2004JD005359, 2005.

860 Viatte, C., Wang, T., Van Damme, M., Dammers, E., Meleux, F., Clarisse, L., Shephard, M. W., Whitburn, S.,  
861 Coheur, P. F., Cady-Pereira, K. E. and Clerbaux, C.: Atmospheric ammonia variability and link with particulate  
862 matter formation: a case study over the Paris area, *Atmos. Chem. Phys.*, 20(1), 577–596, doi:10.5194/acp-20-  
863 577-2020, 2020.

864 Wang, T., Song, Y., Xu, Z., Liu, M., Xu, T., Liao, W., Yin, L., Cai, X., Kang, L., Zhang, H. and Zhu, T.: Why is  
865 the Indo-Gangetic Plain the region with the largest NH<sub>3</sub> column in the globe during pre-monsoon and monsoon  
866 seasons?, *Atmos. Chem. Phys.*, 20(14), 8727–8736, doi:10.5194/acp-20-8727-2020, 2020.

867 Wesely, M. L.: Parameterization of surface resistances to gaseous dry deposition in regional-scale numerical  
868 models, *Atmos. Environ.*, 23(6), 1293–1304, doi:10.1016/0004-6981(89)90153-4, 1989.

869 Whitburn, S., Damme, M. Van, Clarisse, L., Bauduin, S., Heald, C. L., Hurtmans, D., Zondlo, M. A., Clerbaux,  
870 C. and Coheur, P.: A flexible and robust neural network IASI-NH<sub>3</sub>, , 6581–6599,  
871 doi:10.1002/2016JD024828.Received, 2016.

872 Wu, J., Kong, S., Wu, F., Cheng, Y., Zheng, S., Yan, Q., Zheng, H., Yang, G., Zheng, M., Liu, D., Zhao, D. and  
873 Qi, S.: Estimating the open biomass burning emissions in central and eastern China from 2003 to 2015 based on  
874 satellite observation, *Atmos. Chem. Phys.*, 18(16), 11623–11646, doi:10.5194/acp-18-11623-2018, 2018.

875 Xu, J. S., He, J., Behera, S. N., Xu, H. H., Ji, D. S., Wang, C. J., Yu, H., Xiao, H., Jiang, Y. J., Qi, B. and Du, R.  
876 G.: Temporal and spatial variation in major ion chemistry and source identification of secondary inorganic  
877 aerosols in Northern Zhejiang Province, China, *Chemosphere*, 179(December 2014), 316–330,  
878 doi:10.1016/j.chemosphere.2017.03.119, 2017.

879 Xu, R. T., Pan, S. F., Chen, J., Chen, G. S., Yang, J., Dangal, S. R. S., Shepard, J. P. and Tian, H. Q.: Half-  
880 Century Ammonia Emissions From Agricultural Systems in Southern Asia: Magnitude, Spatiotemporal  
881 Patterns, and Implications for Human Health, *GeoHealth*, 2(1), 40–53, doi:10.1002/2017gh000098, 2018.

882 Xu, W., Zhang, L. and Liu, X.: A database of atmospheric nitrogen concentration and deposition from the  
883 nationwide monitoring network in China, , (December 2018), 2–7, 2019.

884 Zhang, X., Liu, J., Han, H., Zhang, Y., Jiang, Z., Wang, H., Meng, L., Li, Y. C. and Liu, Y.: Satellite-Observed  
885 Variations and Trends in Carbon Monoxide over Asia and Their Sensitivities to Biomass Burning, *Remote*

Sens., 12(5), 830, doi:10.3390/rs12050830, 2020.

Zhang, Y., Dore, A. J., Ma, L., Liu, X. J., Ma, W. Q., Cape, J. N. and Zhang, F. S.: Agricultural ammonia emissions inventory and spatial distribution in the North China Plain, *Environ. Pollut.*, 158(2), 490–501, doi:10.1016/j.envpol.2009.08.033, 2010.

Zhao, B., Wang, S. X., Liu, H., Xu, J. Y., Fu, K., Klimont, Z., Hao, J. M., He, K. B., Cofala, J. and Amann, M.: NO<sub>x</sub> emissions in China: Historical trends and future perspectives, *Atmos. Chem. Phys.*, 13(19), 9869–9897, doi:10.5194/acp-13-9869-2013, 2013.

Zheng, J., Hu, M., Du, Z., Shang, D., Gong, Z., Qin, Y., Fang, J., Gu, F., Li, M., Peng, J., Li, J., Zhang, Y., Huang, X., He, L., Wu, Y. and Guo, S.: Influence of biomass burning from South Asia at a high-altitude mountain receptor site in China, *Atmos. Chem. Phys.*, 17(11), 6853–6864, doi:10.5194/acp-17-6853-2017, 2017.

Zhou, Y., Zhang, Y., Tian, D. and Mu, Y.: Impact of dicyandiamide on emissions of nitrous oxide, nitric oxide and ammonia from agricultural field in the North China Plain, *J. Environ. Sci. (China)*, 40, 20–27, doi:10.1016/j.jes.2015.08.016, 2016.

Zhu, L., Henze, D. K., Bash, J. O., Cady-Pereira, K. E., Shephard, M. W., Luo, M. and Capps, S. L.: Sources and Impacts of Atmospheric NH<sub>3</sub>: Current Understanding and Frontiers for Modeling, Measurements, and Remote Sensing in North America, *Curr. Pollut. Reports*, 1(2), 95–116, doi:10.1007/s40726-015-0010-4, 2015.

## FIGURE CAPTIONS

**Figure 1. Spatial distribution of total  $\text{NH}_3$  emissions ( $\times 10^{10} \text{ kg m}^{-2} \text{ s}^{-1}$ ) over Asia. Data are shown at  $0.1^\circ \times 0.1^\circ$  grid resolution from Hemispheric Transport of Air Pollution version-2 (HTAP-v2) emission inventory. The solid rectangles indicate the Indo-Gangetic plain, IGP ( $20^\circ\text{N}$ - $32^\circ\text{N}$ ,  $70^\circ\text{E}$ - $95^\circ\text{E}$ ) and the North China Plain, NCP ( $30^\circ\text{N}$ - $40^\circ\text{N}$ ,  $110^\circ\text{E}$ - $120^\circ\text{E}$ ).**

**Figure 2. Monthly variation of anthropogenic (HTAP-v2) ( $\text{molecules cm}^{-2} \text{ s}^{-1}$ ) (top), Biomass Burning (GEFED-v3) ( $\text{molecules cm}^{-2} \text{ s}^{-1}$ ) (middle) and Soil (CESM) ( $\text{molecules cm}^{-2} \text{ s}^{-1}$ ) (bottom)  $\text{NH}_3$  emission averaged from Indo-Gangetic plain ( $20^\circ\text{N}$ - $32^\circ\text{N}$ ,  $70^\circ\text{E}$ - $95^\circ\text{E}$ ) and the North China Plain ( $30^\circ\text{N}$ - $40^\circ\text{N}$ ,  $110^\circ\text{E}$ - $120^\circ\text{E}$ ).**

**Figure 3. Geographical locations of surface  $\text{NH}_3$  observational sites (69 locations) from the air quality automatic monitoring network operated by the Central Pollution Control Board (CPCB, 2020), India and observational sites (32 locations) from Nationwide Nitrogen Deposition Monitoring Network (NNDMN) operated by China Agricultural University, China.**

**Figure 4. Spatial distributions annual mean  $\text{NH}_3$  ( $\times 10^{16} \text{ molecules cm}^{-2}$ ) total columns over Asia for the year 2010. (a) Simulated by MOZART-4, (b) from the IASI satellite observations and (c) spatial difference between MOZART-4 and IASI.**

**Figure 5. (a) Scatter plot between annual averaged IASI and MOZART-4 simulated  $\text{NH}_3$  ( $\times 10^{16} \text{ molecules cm}^{-2}$ ) total columns over IGP, South Asia (rectangle:  $20^\circ\text{N}$ - $32^\circ\text{N}$ ,  $70^\circ\text{E}$ - $95^\circ\text{E}$ ) and (b) Scatter plot between annual averaged IASI and MOZART-4 simulated  $\text{NH}_3$  ( $\times 10^{16} \text{ molecules cm}^{-2}$ ) total columns over NCP, East Asia (rectangle:  $30^\circ\text{N}$ - $40^\circ\text{N}$ ,  $110^\circ\text{E}$ - $120^\circ\text{E}$ ).**

**Figure 6. Seasonal  $\text{NH}_3$  total columns distribution ( $\times 10^{16} \text{ molecules cm}^{-2}$ ) in 2010 (left) simulated by MOZART-4, (middle) measured by IASI satellite and (right) spatial differences between MOZART-4 and IASI during (top to bottom) winter (DJF) spring (MAM) summer (JJA) and autumn (SON) seasons.**

**Figure 7. Daily vertical distribution of distribution of  $\text{NH}_3$  (ppb) averaged over IGP South Asia ( $20^\circ\text{N}$ - $32^\circ\text{N}$ ,  $70^\circ\text{E}$ - $95^\circ\text{E}$ ) (left) and daily mean Planetary Boundary Layer height (PBLH in meters) averaged over IGP South Asia ( $20^\circ\text{N}$ - $32^\circ\text{N}$ ,  $70^\circ\text{E}$ - $95^\circ\text{E}$ ) (right).**

**Figure 8. (a) Comparison between monthly averaged IASI and MOZART-4 simulated  $\text{NH}_3$  ( $\times 10^{16} \text{ molecules cm}^{-2}$ ) total columns over IGP South Asia ( $20^\circ\text{N}$ - $32^\circ\text{N}$ ,  $70^\circ\text{E}$ - $95^\circ\text{E}$ ), (b) Comparison of monthly averaged IASI and MOZART-4 simulated  $\text{NH}_3$  ( $\times 10^{16} \text{ molecules cm}^{-2}$ ) total columns over NCP East Asia ( $30^\circ\text{N}$ - $40^\circ\text{N}$ ,  $110^\circ\text{E}$ - $120^\circ\text{E}$ ) (bar indicates standard error of 88 and 35 pixels in IGP and NCP respectively).**

**Figure 9.** (a) Scatter plot between annual averaged surface observations from 69 monitoring sites (Fig. 2) over South Asia and MOZART-4 simulated surface  $\text{NH}_3$  ( $\mu\text{g m}^{-3}$ ) (992 hPa) interpolated at the locations of 69 sites (b) Comparison between monthly mean surface observations from 69 monitoring sites and MOZART-4 simulated monthly mean  $\text{NH}_3$  ( $\mu\text{g m}^{-3}$ ) concentration interpolated at the locations of 69 sites over South Asia.

**Figure 10.** (a) Scatter plot between annual averaged surface observations from 32 monitoring sites (Fig. 2) over East Asia and MOZART-4 simulated surface  $\text{NH}_3$  ( $\mu\text{g m}^{-3}$ ) (992 hPa) interpolated at the locations of 32 sites (b) Comparison between monthly mean surface observations from 32 monitoring sites and MOZART-4 simulated monthly mean  $\text{NH}_3$  ( $\mu\text{g m}^{-3}$ ) concentration interpolated at the locations of 32 sites over East Asia.

**Figure 11.** MOZART-4 simulated spatial distribution of annual averaged (a) total sulphate aerosol ( $\times 10^9$  ppb), (b) total Ammonium aerosol ( $\times 10^9$  ppb), (c)  $\text{NO}_x$  total columns ( $\times 10^{16}$  molecules  $\text{cm}^{-2}$ ) and (d) total ammonium nitrate aerosol ( $\times 10^9$  ppb) over Asia.

## TABLES

**Table 1 Model performance statistics for NH<sub>3</sub> total columns over Asia from IASI and MOZART-4 simulations for the year 2010**

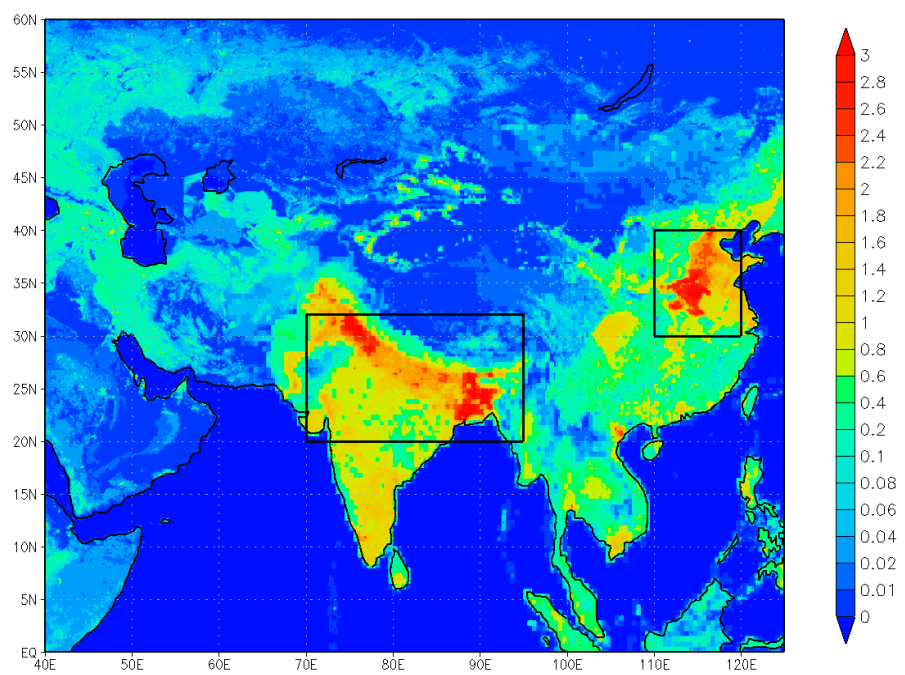
Statistics indicator	IGP, South Asia	NCP, East Asia
Mean (Model-IASI ) ( $\times 10^{16}$ molecules $\text{cm}^{-2}$ )	0.68	-0.24
Normalized Mean Bias (NMB)	0.38	-0.35
Variance ( $\times 10^{16}$ molecules $\text{cm}^{-2}$ )	1.39	-0.83
Root Mean Square Error (RMSE) ( $\times 10^{16}$ molecules $\text{cm}^{-2}$ )	0.125	0.05
Correlation Coefficient (r)	0.81	0.90

**Table 2 Model performance statistics for NH<sub>3</sub> concentration over East and South Asia from MOZART-4 simulations and observational network for the year 2010**

Statistics indicator	IGP, South Asia	NCP, East Asia
Mean (Model-Observations) ( $\mu\text{g m}^{-3}$ )	-13.47	3.1
Normalized Mean Bias (NMB)	0.44	-0.46
Variance ( $\mu\text{g m}^{-3}$ )	-0.629	-0.88
Root Mean Square Error (RMSE) ( $\mu\text{g m}^{-3}$ )	1.91	0.728
Correlation Coefficient (r)	0.82	0.65

1026 **Figure 1**

1027



1028

1029

1030

1031

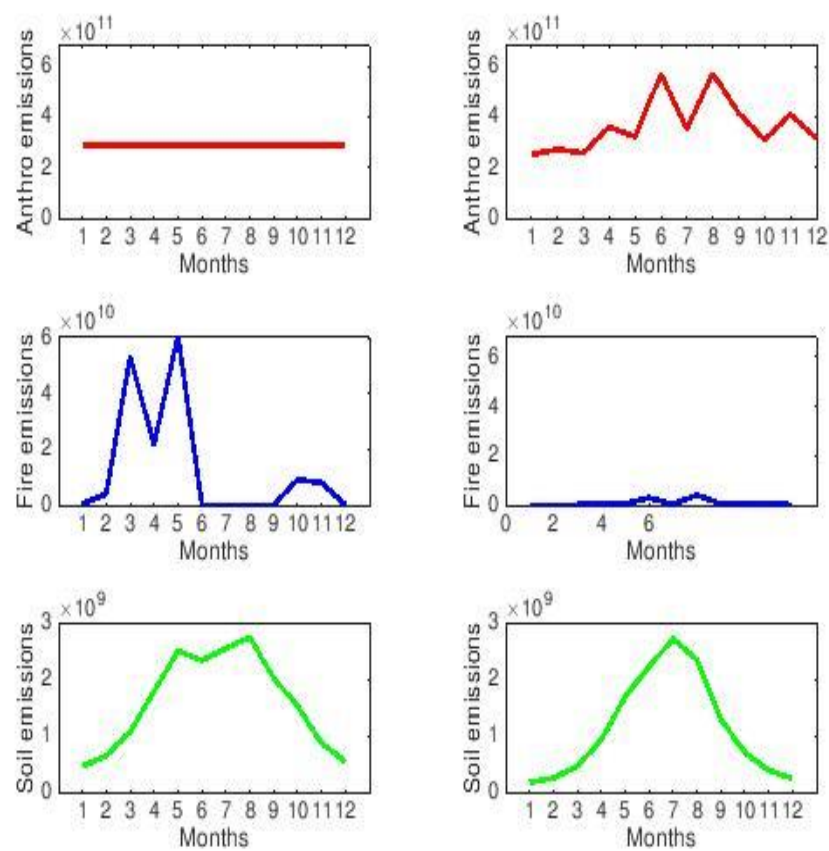
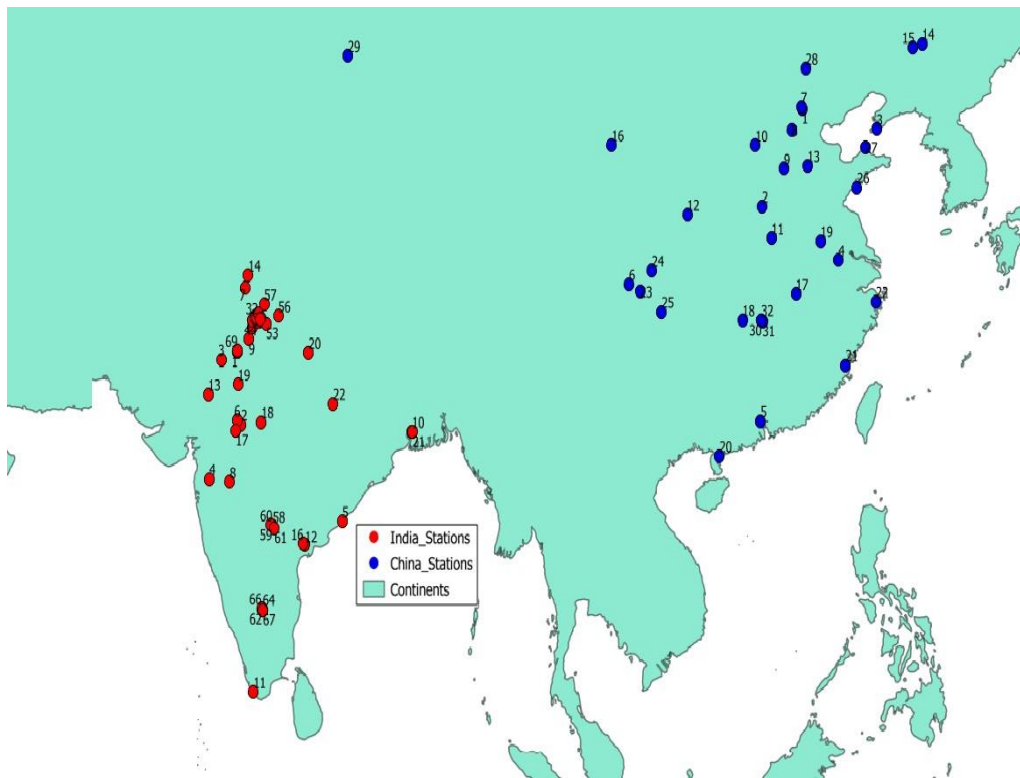
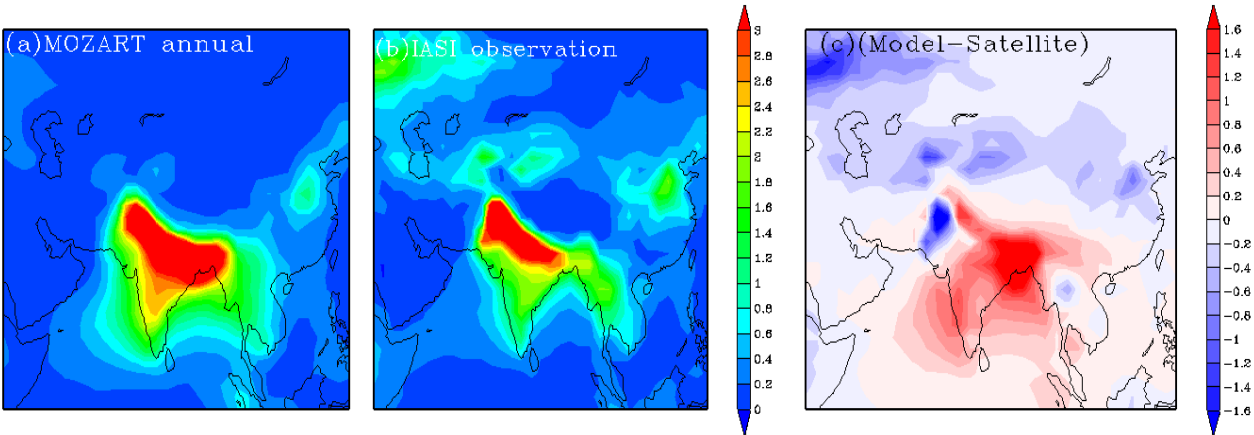


**Figure 3**



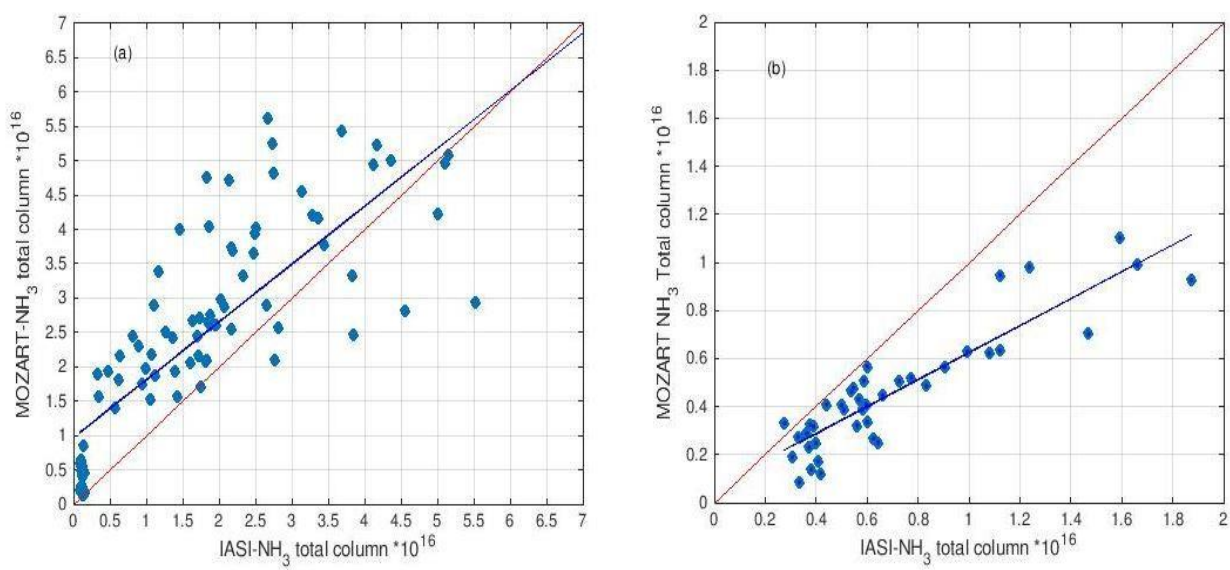
1054 **Figure 4**



1055  
1056  
1057  
1058  
1059

1060 **Figure 5**

1061

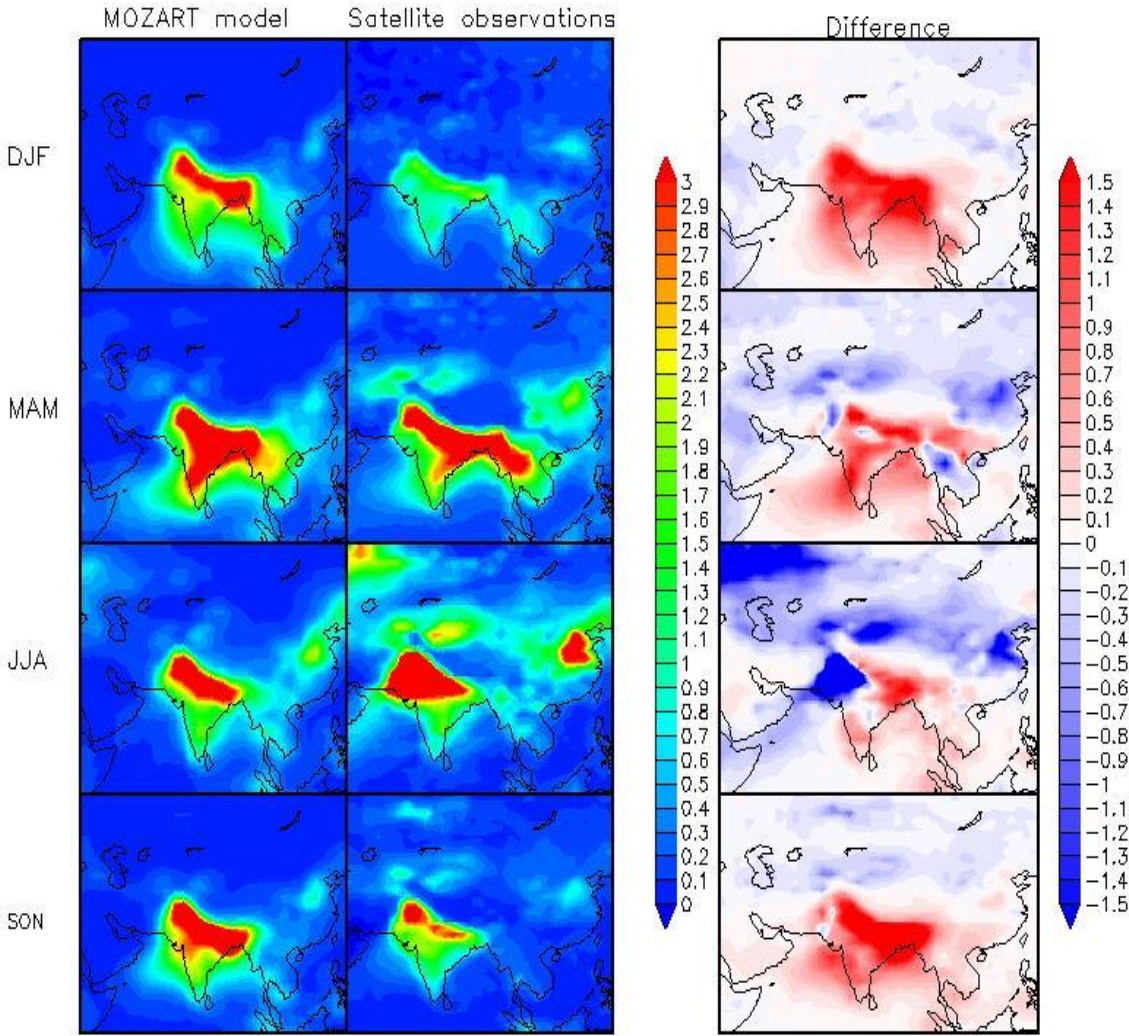


1062

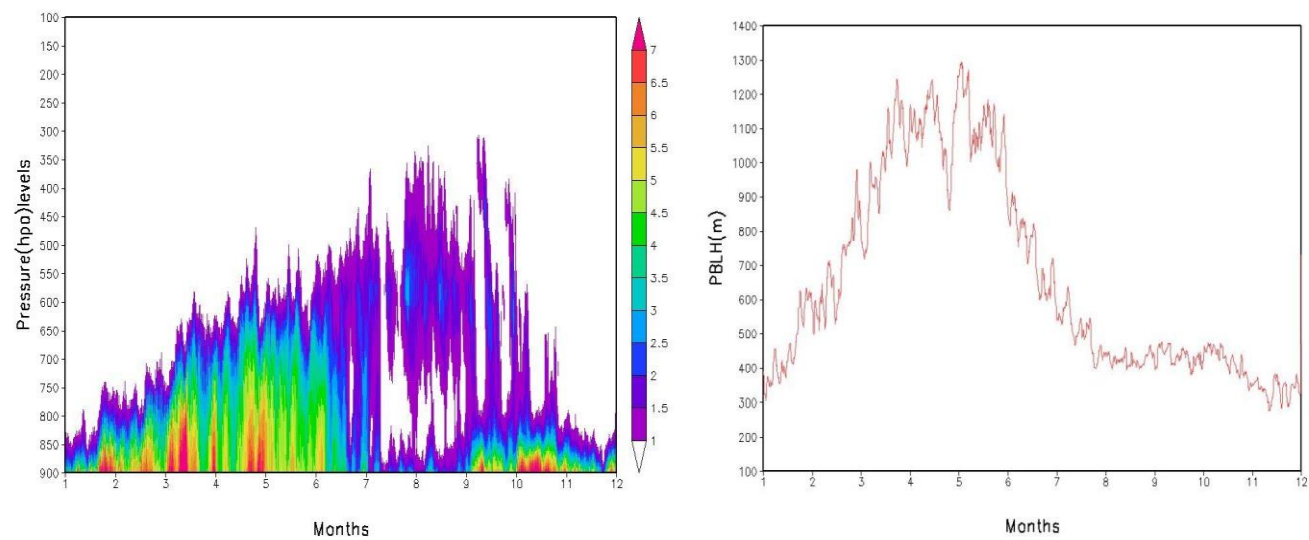
1063

1064

Figure 6



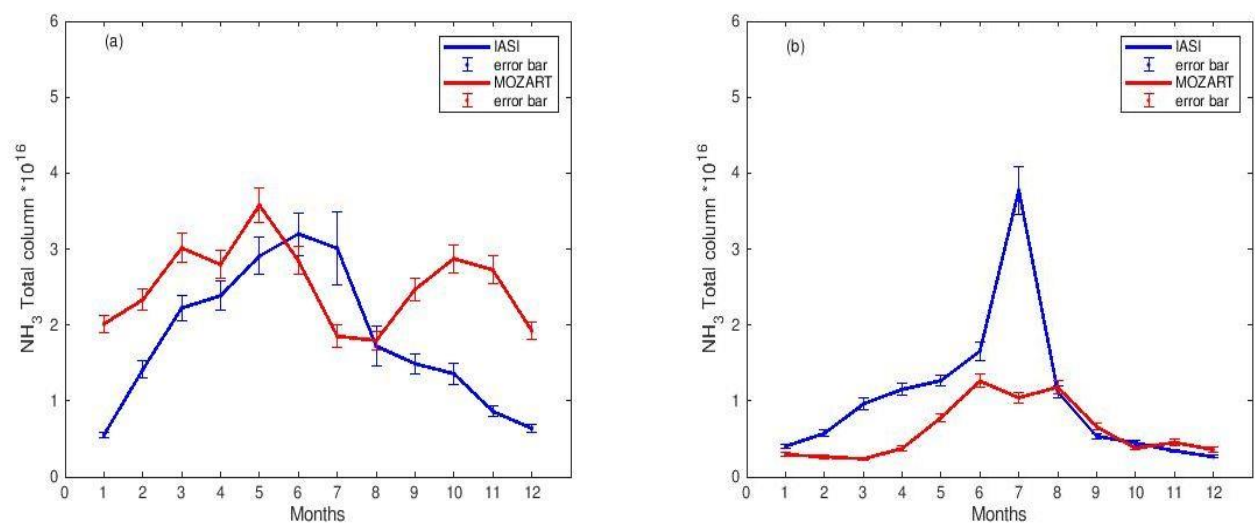
1075 **Figure 7**



1080

1085

Figure 8



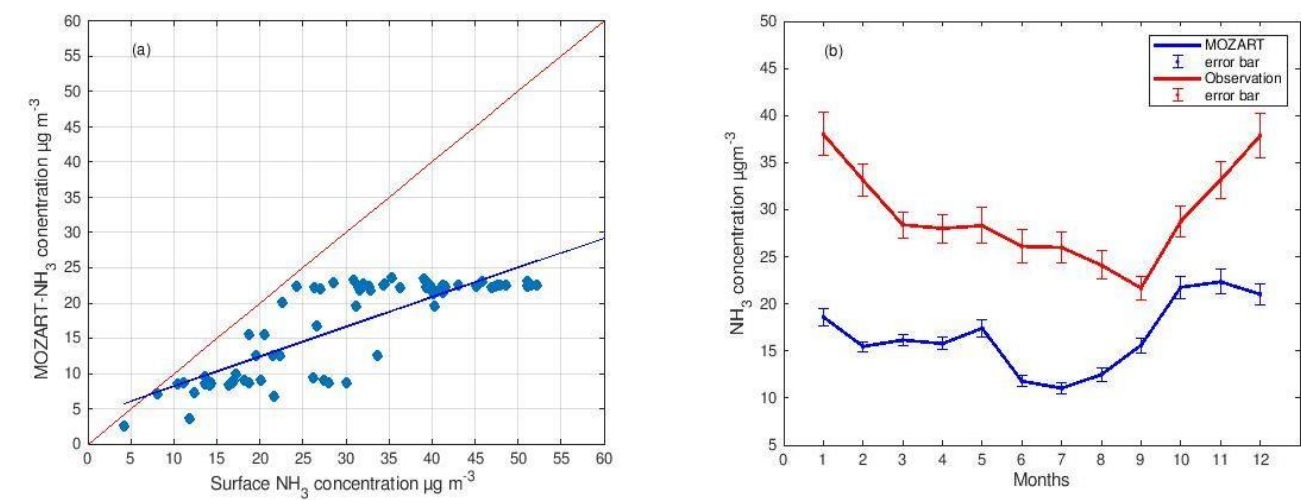
1090

1095

1100

1105

Figure 9

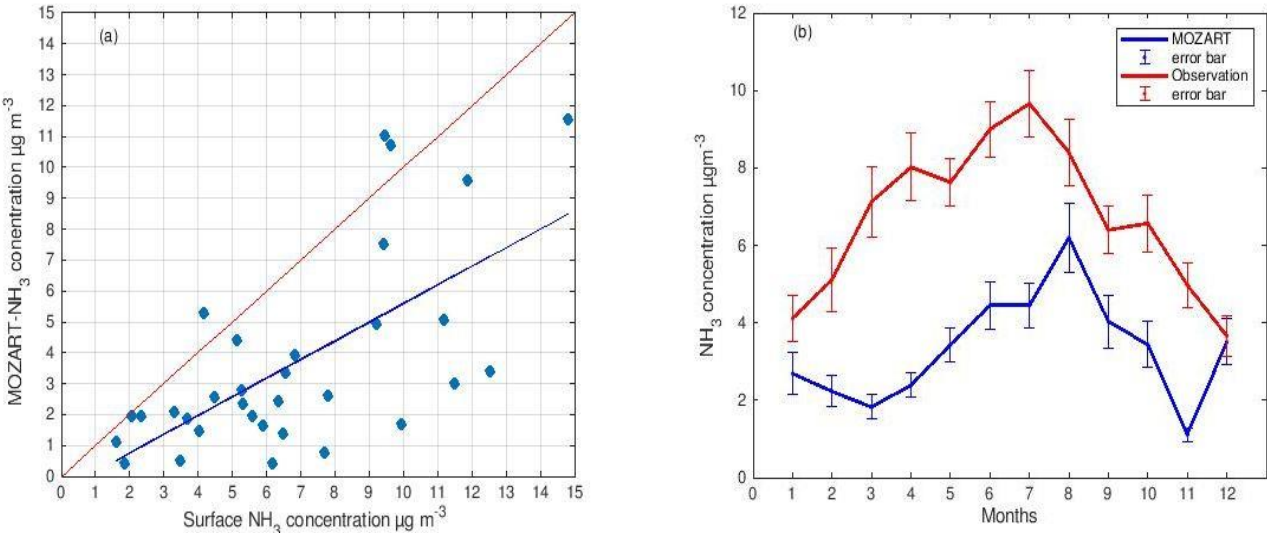


1110

1115

1120

Figure 10



1125

1130

1135

